DOKUZ EYLÜL UNIVERSITY
GRADUATE SCHOOL OF NATURAL AND APPLIED SCIENCES

INVESTIGATION OF PERFORMANCE OF VACUUM COOLING TECHNOLOGY FOR THE FOOD PROCESSING INDUSTRY AND ENERGY STORAGE

by
Murat PİRİ

Temmuz, 2022
İZMİR

INVESTIGATION OF PERFORMANCE OF VACUUM COOLING TECHNOLOGY FOR THE FOOD PROCESSING INDUSTRY AND ENERGY STORAGE

A Thesis Submitted to the
Graduate School of Natural and Applied Sciences of Dokuz Eylül University
In Partial Fulfillment of the Requirements for the Degree of Master of Science
in Mechanical Engineering, Thermodynamics Program

by

Murat PİRİ

Temmuz, 2022
İZMİR

M.Sc THESIS EXAMINATION RESULT FORM

We have read the thesis entitled "**INVESTIGATION OF PERFORMANCE OF VACUUM COOLING TECHNOLOGY FOR THE FOOD PROCESSING INDUSTRY AND ENERGY STORAGE**" completed by **MURAT PİRİ** under supervision of **PROF.DR. AYTUNÇ EREK** and we certify that in our opinion it is fully adequate, in scope and quality, as a thesis for the degree of Master of Science.

……………………………………………

Prof. Dr. Aytunç EREK

Supervisor

……………………………………………

Assoc. Prof. Dr. Mehmet Akif EZAN

(Jury Member)

……………………………………………

Assoc. Prof. Dr. Mustafa ASKER

(Jury Member)

Prof. Dr. Okan FISTIKOĞLU

Director

Graduate School of Natural and Applied Sciences

ACKNOWLEDGEMENT

Foremost, I present my sincere gratitude to my advisor Prof. Dr. Aytunç EREK, for the patient guidance, continuous support, encouragement, patience and motivation from the beginning of this research. I am proud to work with him, he teaches me to gain a different perspective on engineering and research.

Besides my advisor, I would like to thanks to Okan GÖK for valuable experience, insightful comments and knowledge for computional fluid dynamics and thermodynamic.

I also express my gratitude to Ezgi YALDIZ, who has a great place in my life and supports me. Most importantly, I am grateful to them for the endless patience, support, and perseverance of my entire family, especially my mother and father.

Murat PİRİ

INVESTIGATION OF PERFORMANCE OF VACUUM COOLING TECHNOLOGY FOR THE FOOD PROCESSING INDUSTRY AND ENERGY STORAGE

ABSTRACT

Nowadays, shelf life and product quality are very important since people have started to use more packed foods. Recent studies have proved that vacuum cooling has great advantages over other cooling technologies. In the first part of this study, the freezing stage of the vacuum cooling process was investigated with the simplified one-dimensional transient analyses which were done in Matlab2020b using the thermal resistance network model approach. Parametric analyses were done by changing design parameters such as; working logic and product weight. Analysis results showed, gradual working logic was better and safer than single-step working logic. The temperature difference between internal air and insulation was lower than 1.5K, but the product core temperature was 4.15K colder. The evaporator capacity was calculated as 150W. In the second part of the study, a rectangular chamber was proposed to improve cooling performance and machine quality. The maximum deformation of cylindrical chamber and a rectangular chamber with two support were found as 1.2mm. The internal air circulation of the machine comparment was investigated seperately. Grills, holes, separators, and diffusers were added to improve internal air circulation and reject warmed air to the ambient. Heat transfer rates through the condenser with and without seperator and diffuser were 4132W and 3200W, respectively, and the performance increased by %29. In the third part of the study, cooling performance of the rectangular chamber was focused. Three different insulation thicknesses (i.e. 40mm, 45mm, and 50mm) were compared based on evaporator temperatures. Due to mechanical and heat gain, 45mm insulation thickness was chosen. The fin on tube evaporator was added to increase system cooling performance and dehumilidate air before vacuum pump. Cooling performance was increased, and also air circulation analyses showed air passing through the evaporator.
Keywords: one-dimensional transient analysis, thermal resistance network, vacuum cooling

GIDA ENDÜSTRİSİNDE VE ENERJİ DEPOLAMADA KULLANILAN VAKUMLU SOĞUTMA TEKNOLOJİSİNİN PERFORMANSININ DEĞERLENDİRİLMESİ

ÖZ

Günümüzde insanlar daha fazla paketli gıda kullanmasıyla birlikte gıda sektöründe raf ömrü ve ürün kalitesi çok önemli hale gelmiştir. Yapılan son çalışmalarda vakumlu soğutmanın işlem süresi ve ürün kalitesi bazında diğer soğutma teknolojilerine göre büyük bir avantajının olduğu kanıtlanmıştır. Bu çalışmanın ilk aşamasında vakumlu soğutmanın dondurma aşaması basitleştirilmiş bir boyutlu zamana bağlı analizi Matlab2020b yazılımı ile incelenmiştir. Parametrik analizler çalışma prensibi ve ürün ağırlığı gibi tasarım parametreleri değiştirilerek yapılmıştır. Değişken kademeli çalışma metodu tek kademeli çalışma metoduna göre daha iyi ve güvenlidir. Sıcaklık farkları olarak, iç ortam hava ve yalıtım sıcaklığı 1.5K, ürünün ana merkezi ise 4.15K daha soğuktur. Buharlaştırıcı kapasitesi 150W olarak hesaplanmıştır. Bu çalışmanın ikini aşamasında soğutma gücünü ve makinenin kalitesini arttırmak için dikdörtgen bir hazne önerilmiştir. Silindir ve dikdörtgen haznelerin en yüksek deplasmanları 1.2mm bulunmuştur. İç hava sirkülasyonunu iyileştirilmesi ve ısınan havanın makineden ortama atılması için kanallar, delikler, ayırıcı ve yönlendiriciler eklenmiştir. Kondenserden geçen ısıl transfer oranı 4132W ve 3200W olarak ayırıcı ve yönlendiricili ile ve ayırıcı ve yönlendiricisiz olarak hesaplan ve bu %29'luk bir performans artışı demektir. Bu çalışmanın üçüncü aşamasında dikdörtgen haznenin soğutma performansına odaklanılmıştır. Buharlaştırıcı sıcaklıkları temel alınarak, üç farklı yalıtım kalınlığı (örn. 40mm, 45mm, 50mm) için analiz yapılmıştır. Mekanik sınırlar ısıl kazançtan dolayı 45mm yalıtım sıcaklığı seçilmiştir. Sistemin soğutma kapasitesinin iyileştirilmesi ve vakum pompası öncesi havanın kurutulması için kanatlı buharlaştırıcı eklenmiştir. Soğutma performansı artmıştır ve ayrıca havanın buharlaştırıcı üzerinden geçtiğini hava akış analizlerinde gösterilmiştir.

Anahtar kelimeler: bir boyutlu zamana bağlı analiz, ısı direnç ağı, vakumlu soğutma

CONTENTS

LIST OF FIGURES

LIST OF TABLES

Page

LIST OF SYMBOLS

C	Thermal capacitance [J/K]
V	Volume [m3]
cp	Specific heat [J/kgK]
h	Heat transfer coefficient [W/m^{2}K]
k	Thermal conductivity [W/mK[
R	Thermal resistance [Ks^{-1}J^{-1}]
Q	Heat tranfer [J]
$\dot{Q}$	Heat transfer rate [W]
T	Temperature [K]
t	Time [s]
TECM	Thermal equivalent circuit method [-]
m	mass [kg]
L	Length [m]
ρ	Density [kg/m^3]

ABBREVIATIONS

pu1	First isolation part (polyurethane)
pu12	Second isolation part (polyurethane)
intair	Internal air
outair	Outer air
intair1	First internal air section
intair2	Second internal air section
product	Product
chmwall	Chamber wall
shelves	Shelves
out	Outlet

CHAPTER ONE
INTRODUCTION

People have started preserving their food since ancient times. The top of the mountains is a great option cause of the low temperature and pressure. Eskimos and other ancient peoples protected their foods under the snow (Meryman H.T, 1976). In 1250-850 B.C., Peruvian ancient people preserved their food under Machu Picchu's low temperature and pressure which leads to sublimation. These people didn’t recognize their foods are freeze-dried. Ancient population carried their food to the mountain where temperature and pressure were low, these conditions are the basic freeze-drying process (Salaman R.N., 1949).

In the most recent studies, in the 20th century, Benedict and Manning have dried animal tissue below 1 atm by the chemical pump. Shackell discovered to preserve biologicals had to be frozen before the drying process, this is the actual freeze-drying process. Later on, Shackell designed a basic system with an electrical pump based on Benedict and Manning's study outcomes. After that, freeze-drying technology improvements accelerated. Coffee was the first freeze-dried product that has been manufactured and it led to the commercial usage of freeze-dryers. The significant historical improvement reported during World War II, blood plasma and penicillin were freeze-dried and it was start point to use this method in the pharmacy industry. This method was used in the Apollo mission on ice cream. Nowadays, freeze-drying methods are used in different industries such as food, pharmacy, space, and museum.

Freeze-drying systems are using the vacuum cooling principle and airblast, water immersion, and slow air are some of the other traditional cooling principles. Vacuum cooling and other cooling methods were compared in terms of thermophysical properties (Donald et al., 2001). Results show the beef product has higher mass reduction and lower thermophysical properties due to high moisture removal with vacuum cooling. Apart from them, the vacuum cooling system has a lower process time which brings energy advantages. Vacuum cooling systems are applicable for other products such as lettuces, fruits and vegetables, fish, bakery products, soup, and sauce. The study showed the wide usage field of vacuum cooling systems, the advantages, and the disadvantages. (Donald & Sun, 2000). Lettuces, fruits, and vegetables are the big fields that use vacuum cooling technology. Lettuce is analyzed thermodynamically and results are satisfied with experimental results (Isik Esref, 2007). Basil temperature was reduced by vacuum cooling and experimental results proved rapid cooling and mass loss (Gunes & Ekren, 2017). Purslane is cooled by a vacuum and convectional cooling system and results showed vacuum cooling is faster but the mass loss is higher (Ozturk et al., 2011). Cherry fruits were analyzed with a vacuum cooling system and results showed vitamin C and titrated acids are higher with respect to usual cold storage (Lomeiko et al., 2019). Analyzing heat and mass transfer is crucial for food industries for product quality and shelf life. In this case, there are some solution methods such as one-dimensional and computational fluid dynamics (CFD). One-dimensional solution methods were built by the mathematical model and results need to compare with experimental results for precision. Vacuum cooling systems are analyzed by mathematical method and heat and mass transfer results are satisfied with experimental results (Wang & Sun, 2002). Another solution method, which is CFD solutions, is also applicable for heat and mass transfer analyses. The core and surface temperature of the product and chilling time are analyzed with the CFD method and the results were met with experimental results (Sun & Hu, 2002), (Wang et al., 2019). Experimental studies are useful to understand the vacuum cooling process, temperatures are not decreasing rapidly, and there are some variations due to phase change and system inconstancy. Experimental results showed deep-dive analysis on temperature variation concerning the temperature of product and process time (Jin T.X, 2005). A vacuum pump is used to reduce pressure inside the chamber but this pressure level is too low to speed up the processing time. At that point, the mechanical properties of the chamber are important. Stainless steel is the best option for other alternatives such as aluminum and copper. Humidity can cause rust inside the chamber so this is another advantage of stainless steel. The shape is another point for uniform temperature and pressure and a cylindrical chamber is the best option

(Zhang et al., 2009). We can see that most commercial freeze-drying machines have a cylindrical chamber.

1.1 Freeze-Drying Process

The freeze-drying system has three processes to complete drying. These are freezing, primary drying, and secondary drying.

1.1.1 Freezing

The freeze-drying systems are using the sublimation principle which is the phase change from solid to gas. Moisture which is water inside the product becomes a solid phase by the freezing process and then turns back to gas with the next process steps.

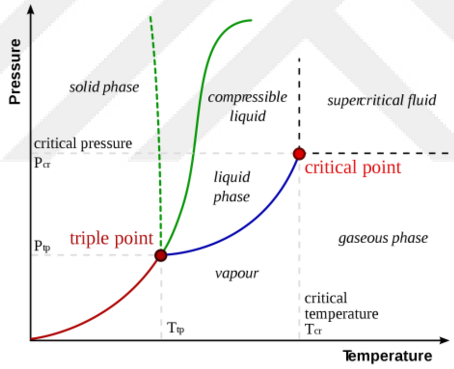

Figure 1.1 Water phase change diagram

Sublimination can occur on the red line which is shown in Figure 1.1. The freezing process is necessary to crystallize the water and solid content of the product. There are several ways to decrease the temperature inside the chamber but there are two types of freezing processes in the field; direct cooling and indirect cooling. Direct cooling is using refrigerant inside the chamber and cooling down the products directly using the refrigerant heat transfer ability but this solution is using for mainly in the pharmacy industry cause products are sealed inside tubes. This system does not apply to the food industry since products are sensitive. An indirect cooling system is the refrigeration cycle in which we are using refrigerant heat transfer benefit by evaporator pipes. This solution is more applicable to the food industry since there is no direct contact between the refrigerant and products.

1.1.2 Primary Drying

Chamber pressure is reduced by a vacuum pump and it is evacuated till reaches the pressure level for sublimation. After the freezing process, most of the moisture creates a layer on the frozen product. Sublimination starts from the layer on the product and water molecules start phase change from solid to vapor and which leads to temperature reduction. Chamber heat is increased by a heater below the shelves to increase the sublimation speed. Most of the moisture exists in the frozen layer of the product and the primary drying process end till the frozen layer evaporate.

1.1.3 Secondary Drying

Most water sublimates during the primary drying but the secondary drying process is necessary to remove the water which is not frozen and most of this water is trapped inside the product. Temperature increases between 10 °C to 35 °C complete drying process. The end temperature is the product packaging temperature.

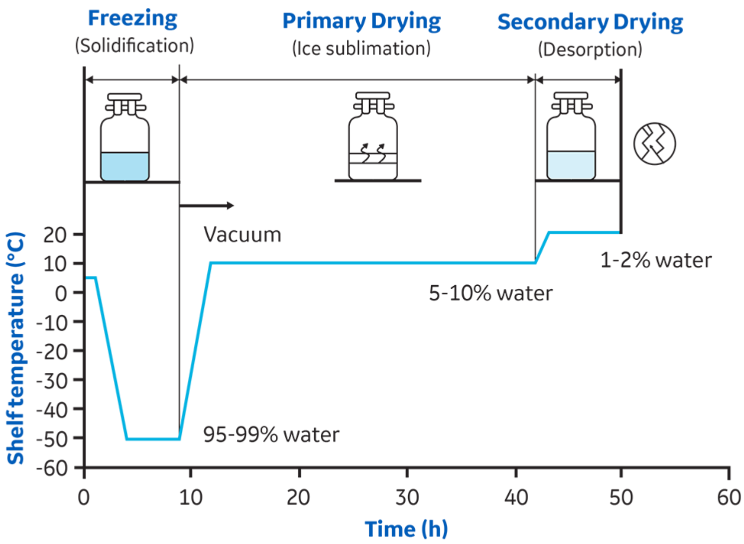

Figure 1.2 Process stages in the pharmacy industry

1.2 Thermal Equivalent Circuit Model

Solution methodology is very important for accurate results and solution duration. This method allows us to solve heat transfer equations similar to electrical circuit problems and possibilities to use electrical circuit solution methods such as Kirchoff.

This method is very applicable for multi-layer models. TECM method is used to calculate transient heat conduction problems with different heat transfer models. The heat exchanger was modeled with the TECM model to observe fluid property change. Results are compared with ε-NTU correlations and they were accurate (Zhao & Chen, 2016). Similarly, internal forced convection in circular tube modeled with TECM and results are aligned with correlations (Ho et al., 2015). Some of the heat exchanger models have many tubes such as borehole heat exchangers which is increasing our model complexity. The borehole heat exchanger model was built with the TECM method with 4 pipes, it solved the transient approach and the results are satisfied with experimental results. (Marcotte and Bernier, 2018), (Dube Kerme & Fung, 2020) TECM model can use in multiple environments such as calculating home thermal system. Commercial office buildings are modeled with a simplified TECM method and the results are accurate with dynamic thermal performance (Wang & Hu, 2005). A similar study was investigated for houses and results were performed on different rooms and wall components. Measured and simulated results were compared and the results were satisfying (Ghiaus & Ahmad, 2019). Another study was done on the scope of house wall bricks to thermal resistance with different methods. Results were analyzed with different sessions and aligned with measured data (Deconinck & Roels, 2016). Al smelting systems which are similar to electronic systems were analyzed with the TECM method with convection, convection, and radiation circuits. System temperatures and heat transfer rates were studied (Zhao et al., 2013). CO2 direct expansion ground source heat pumps are used for heating and cooling homes and small stores. 1D modeling is very popular to solve this kind of system and the study showed that the TECM method is also applicable. The model was created with TECM and the results are satisfied with expectations (Nguyen & Eslami-Nejad, 2019). Battery temperature is crucial for system maintenance and performance. These systems can have many layers when we build a heat transfer model. TECM has accurate results to experimental data (Gan et al., 2018). In another study, a lithium-ion battery cooling system was designed with heat pipes and a system modeled with TECM, 1D, and 3D CFD methods. Results proved the alignment between TECM with 1D and 3D analysis results (Greco et al., 2014). TECM model may use for heat conduction with multi-layer models but data points need to be more frequent as similar as meshing approaches. The study proposed an improved data point scenario that can give accurate results with a short process time (He et al, 2017). This method is feasible with small and complex systems such as multi-chip modules. Heat transfer model created for multi-chip model with TECM and aim was the analyze temperature rise transiently. Analysis was done considering natural convection, thermal radiation, and thermal diffusion by conduction, and results satisfied with measured temperatures (Ishizuka et al., 2011). In another study, an electrical circuit was modeled with the TECM method. Results were compared with 3D results, temperatures were similar. Heat transfer problems are essential for the aerospace industry and these models can be complex as multi-chips. The satellite temperature distribution is crucial for system performance. Satelite heat transfer modeled with TECM and solved with software transient and steady-state stages, results are acceptable (Liu et al., 2009).

1.3 Structure of the Thesis

This thesis is comprised of five chapters, as follows.

- The first section named "Introduction", summarized details of the history and field of usage of vacuum cooling systems, with three-stage of the system. Explained the building of a numerical model based on the TECM method. Recent studies related to vacuum cooling and the TECM method. Also, the thesis structure was given.
- The second section provides the created model with layers; insulation, chamber wall, shelves, internal air, and products with material and dimension details.

TECM method application for this simplified quarter chamber, equations for temperature distribution, absorbed heat, and evaporator capacity. Equations were solved with the Crank-Nicholson method which is a combined method of implicit and Euler’s method.

- The third part mentioned the results of the second section with different working logic which are gradual and one-step. Gradual working logic is general compressor working logic and one-step working logic is the mean temperature of gradual logic. Other main points, product weight (3kg, 4kg, and 5kg), absorbed heat, and evaporator capacity analyzed for both working logic.
- In the fourth section, a rectangular chamber is designed as an alternative chamber. In other to understand the pros and cons mechanical and computational fluid dynamic (CFD) analyses were done. These analyses were done for the basic purpose of the new design, not at the system level.
- Chapter five summarizes the target of the thesis, remarks, and literary contributions.
- In Appendix-1, the nomenclature is given.

CHAPTER TWO
ONE DIMENSIONAL MODELLING AND TECM METHOD OF CYLINDRICAL CHAMBER

2.1 Model Introduction

An example chamber is shown in Fig 2.1a. Due to symmetry of the model, a quarter of the chamber is modelled as in Fig. 2.1b. This model includes insulation, chamber wall, shelves and other metal equipment, internal air, and product model. For better and more accurate results, evaporator pipes are neglected and refrigerant temperature is defined as the outer chamber wall.

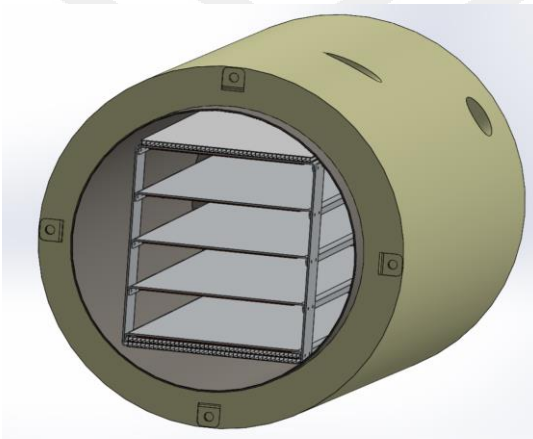

(a)

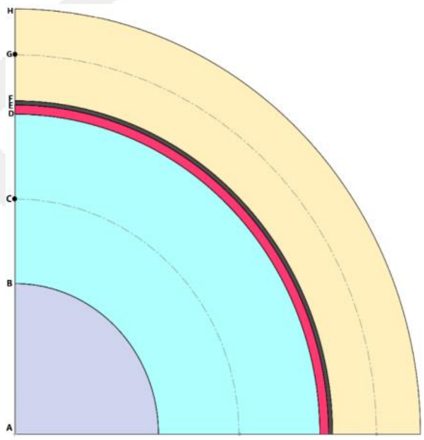

(b)

Figure 2.1 An example chamber (a) and simplified quarter model (b)

The simplified model includes the yellow part as the insulation, the gray part as the chamber wall, the red part is simulating the shelves and other metal components inside the chamber. Shelves and other metal components are metal that can create resistance between the chamber wall and internal air. These parts are modeled as between the chamber wall and internal air. The light blue part is the internal air inside the chamber, the light purple part is modeled as the product. Internal air (point C) and insulation temperatures (point G) defined the middle of the part and equations were created accordingly. Product and internal air dimensions are variable cause they are changing by product weight. Dimensions and coordinates details are given in Table 2.1.

Table 2.1 Model Description by sections

	Material	**Thickness**	**Coordinates**
Product	Apple	Variable	A-B
Internal Air	Air	Variable	B-D
Shelves	Stainless Steel	4.45 mm	D-E
Chamber Wall	Stainless Steel	2 mm	E-F
Insulation	Polyurethane	45 mm	F-H

Table 2.2 Thermopyshical properties of sections

	Specific Heat (J/kgK)	**Density (kg/m^3)**	**Thermal Conductivity (W/mK)**
Product	3690	845	0.427
Insulation	2677.5	23.5	0.049
Shelves	460.548	7740	14.4
Chamber Wall	460.548	7740	14.4

The product is assumed as an apple for this model. Thermophysical properties are taken from experimental results for the golden delicious kind and unfrozen stage (Ramaswamy & Tung, 1981). Specific heat experimental results Polyurethane is the most common material of cooling system manufacturers cause of useful and economic reasons. Thermodynamic properties are changing depends on the phase of insulation but there we considered insulation is solid. The study compared literature data with experimental results with different types of polyurethanes and the results are satisfied (Pau et al, 2013). Thermophysical properties considered the average of the values for this study. Density was investigated in another study and measured data was used in this study (Prasad et al, 2009).

2.2 TECM Method Application

In order to use the TECM method, we need to create the differential equations of heat transfer. Equations can create for each section according to the study done for buildings (Wang & Hu, 2005). TECM method applied to this model and shown in Fig. 2.2.

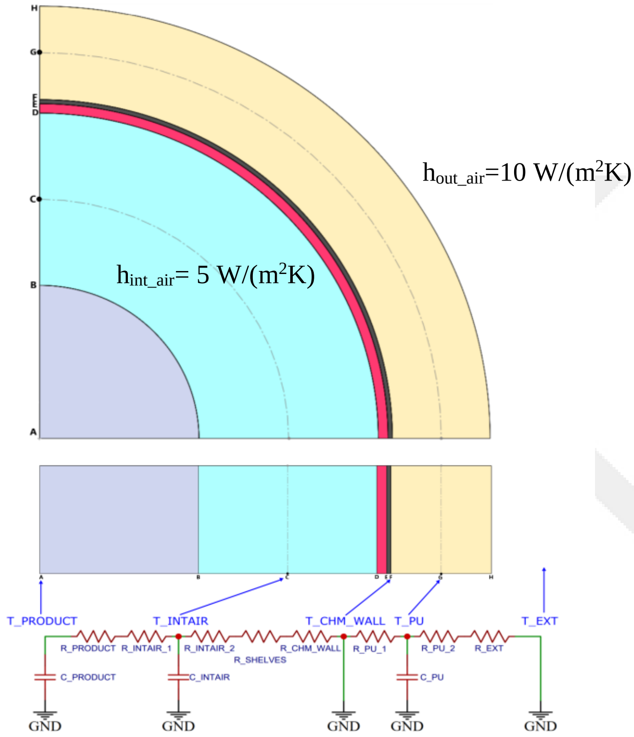

Figure 2.2 TECM Model Application

The insulation temperature (Point G on Fig 2.2) depends on chamber wall and external air temperature, internal air temperature (Point C on Fig 2.2) depends on the chamber wall and product temperature, and product core temperature (Point A in Fig 2.2) depends on internal air temperature. The model assumptions are;

- h_{int_air} and h_{out_air} are 5 and 10 (Kosky et al., 2013), constantly.
- Radiative heat transfer is neglected.
- T_EXT and T_PRODUCT are constant 298K and 293K, initially.
- Product thickness (Point A-B) is variable according to product weight.

Thermal capacitance general equation and for zones,

$$C = V\rho c_p \tag{2.1}$$

$$C_{PU} = V_{PU}\rho_{PU}c_{p_{PU}} \tag{2.2}$$

$$C_{IntAir} = V_{intair}\rho_{intair}c_{p_{intair}} \tag{2.3}$$

$$C_{product} = V_{product}\rho_{product}c_{p_{product}} \tag{2.4}$$

Temperature distribution equations,

$$C_{pu}\frac{dT_{pu}(t)}{dt} = \frac{T_{chmwall} - T_{pu}(t)}{R_{pu_1}} - \frac{T_{ext} - T_{pu}(t)}{R_{ext} + R_{pu_2}} \tag{2.5}$$

$$C_{intair}\frac{dT_{intair}(t)}{dt} = \left\{\begin{array}{c}\left(\frac{T_{chmwall}(t) - T_{intair}(t)}{R_{intair_2} + R_{chmwall} + R_{shelves}}\right) \\ -\left(\frac{T_{intair}(t) - T_{product}(t)}{R_{intair_1} + R_{product}}\right)\end{array}\right\} \tag{2.6}$$

Thermal capacitance is known as the heat capacity of a section and this approach specifically was used in the following studies related to boreholes heat exchangers (Marcotte and Bernier, 2018), heat transfer systems for battery modules (Gan et al., 2018), Commercial buildings thermal performance calculation (Wang & Hu, 2005).

$$\begin{aligned} T_{pu}{}^{t+1} = T_{pu}{}^{t} &+ \left\{\left[\left(\frac{T_{chmwall}{}^{t} - T_{pu}{}^{t}}{C_{pu}R_{pu_1}}\right) - \left(\frac{T_{ext}{}^{t} - T_{pu}{}^{t}}{C_{pu}(R_{ext} + R_{pu_2})}\right)\right]\right. \\ &+ \left.\left[\left(\frac{T_{chmwall}{}^{t+1} - T_{pu}{}^{t+1}}{C_{pu}R_{pu_1}}\right) - \left(\frac{T_{ext}{}^{t+1} - T_{pu}{}^{t+1}}{C_{pu}(R_{ext} + R_{pu_2})}\right)\right]\right\}\frac{\Delta t}{2} \end{aligned} \tag{2.7}$$

$$\begin{aligned} T_{intair}{}^{t+1} = T_{intair}{}^{t} & \\ &+ \left\{\left[\left(\frac{T_{chmwall}{}^{t} - T_{intair}{}^{t}}{C_{intair}(R_{intair_2} + R_{chmwall} + R_{shelves})}\right)\right.\right. \\ &- \left.\left(\frac{T_{intair}{}^{t} - T_{product}{}^{t}}{C_{intair}(R_{intair_1} + R_{product})}\right)\right] \\ &+ \left.\left[\left(\frac{T_{chmwall}{}^{t+1} - T_{pu}{}^{t+1}}{C_{pu}R_{pu_1}}\right) - \left(\frac{T_{ext}{}^{t+1} - T_{pu}{}^{t+1}}{C_{pu}(R_{ext} + R_{pu_2})}\right)\right]\right\}\frac{\Delta t}{2} \end{aligned} \tag{2.8}$$

$$\begin{aligned} T_{product}{}^{t+1} = T_{product}{}^{t} & \\ &+ \left\{\left[\left(\frac{T_{intair}{}^{t} - T_{product}{}^{t}}{C_{product}(R_{product} + R_{intair_1})}\right)\right]\right. \\ &+ \left.\left[\left(\frac{T_{intair}{}^{t+1} - T_{product}{}^{t+1}}{C_{product}(R_{product} + R_{intair_1})}\right)\right]\right\} \end{aligned} \tag{2.9}$$

Crank-Nicholson method is the combined method of implicit and Euler's method which is more accurate. A similar approach was done to solve on study for the U-tube borehole system (Kerme and Fung, 2020).

Equations calculation flow is shown in Fig 2.3. Inputs and outputs are T_CHM_WALL, T_EXT, and T_INTAIR, T_PRODUCT, T_PU. T_CHM_WALL was taken related to working logic, T_EXT assumed as 298K.

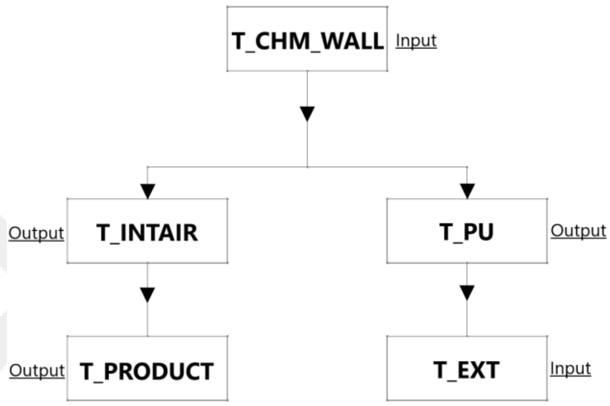

Figure 2.3 Equation calculation flow

2.3 TECM Method Results

Insulation zone temperature changes by external air and chamber wall temperatures, external air assumed as 298K, constantly. Insulation temperature depends on one variable. Internal air temperature changes by chamber wall and product temperatures, also product temperature changes by internal air temperature, so that there are two equations and two unknowns, equation system is solved as a linear equation system. Equations are solved with the iterative method to improve results accuracy. Equation system solved by Matlab 2020b software.

2.3.1 Gradual and Single-Step Working Logic

Chamber wall temperature was taken by experimental results and the average of experimental results. This parametric study aims to show the benefit of gradual working with respect to a single-step working algorithm. Gradual working logic contains three periods; first, second and stable. The first run takes about 5hr and the compressor stops, the second run takes about 5hr and the compressor pressure is less to achieve a colder temperature. The stable run takes about 10hr and we have the warmest temperature. The single-step working temperature is 240K, calculated as the mean temperature of the last period. Working logics are shown in Fig 2.4.

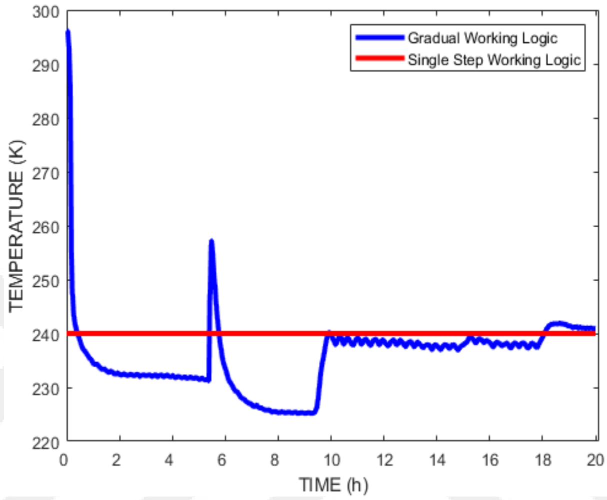

Figure 2.4 Gradual and single-step working logic

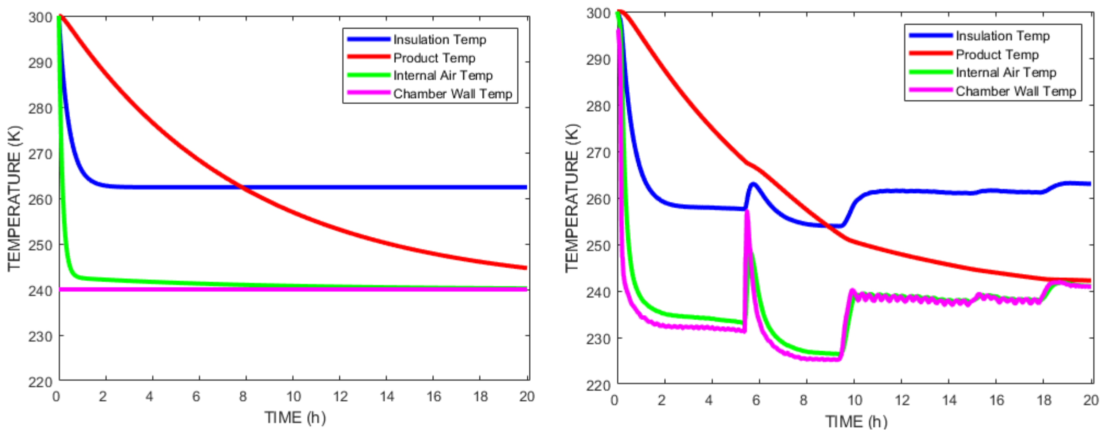

(a) (b)

Figure 2.5 Temperature comparison of single-step (a) and gradual (b) working logic

In this comparison study, the product weight was assumed as 5kg. Temperature results calculated by Eqs. (2.7)-(2.9). Product weight accepted as 5kg. Gradual and single-step working logics temperature are shown in Fig 2.5. Temperature dynamics change more rapidly with gradual working logic that creates fluctuations since there are no fluctuations with single-step logic. The mean temperature of the last hour was compared. Gradual working logic achieves lower temperatures during the first and second periods which we reduced temperatures of internal air, product, and insulation.

Table 2.3 Temperature results of working logics

	Internal Air Temperature (K)	**Product Temperature (K)**	**Insulation Temperature (K)**
Gradual	239.07	247.58	261.50
Single-step	240.45	251.73	262.41

2.3.2 Product Weight Comparison

Another important point is the system capacity. This parametric study demonstrates product weight difference impact on temperatures. As in Fig 2.6 and Fig 2.7 more weight is hard to freeze.

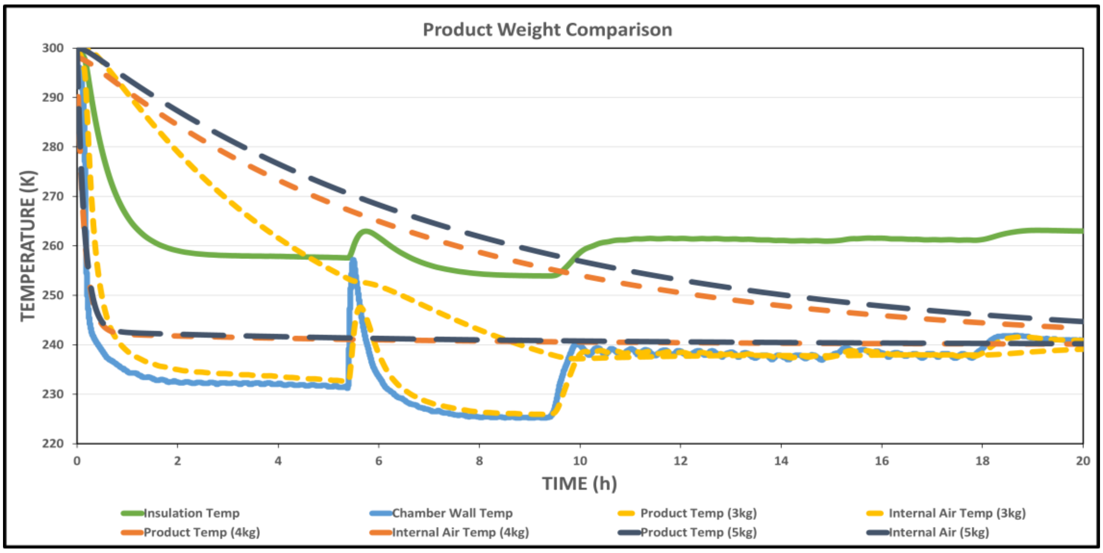

(a)

Figure 2.6 Gradual working logic temperature comparison (a), last one-hour temperatures (b)

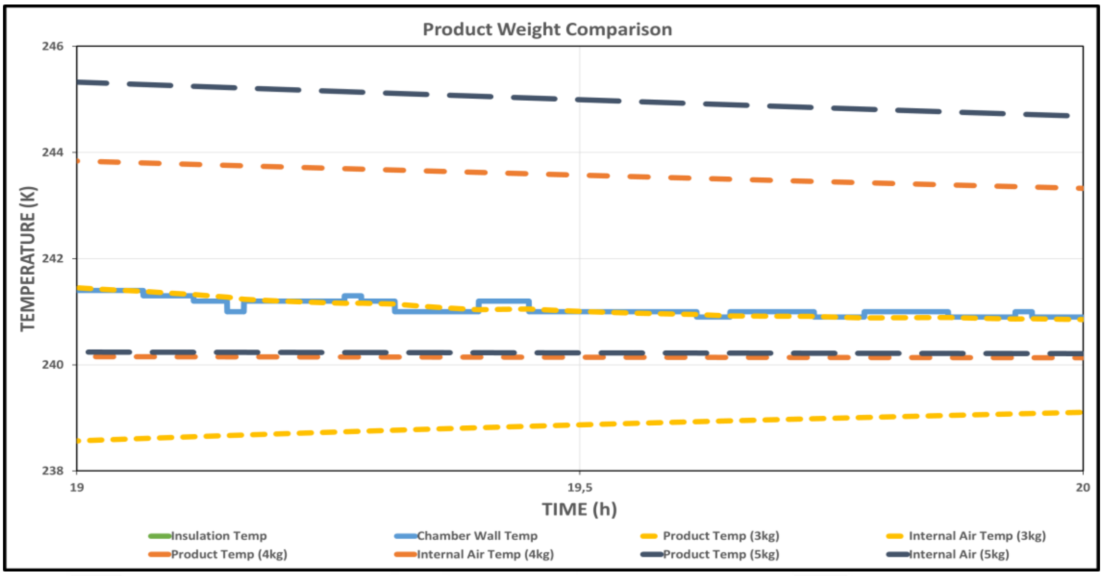

(b)

Figure 2.6 Continues

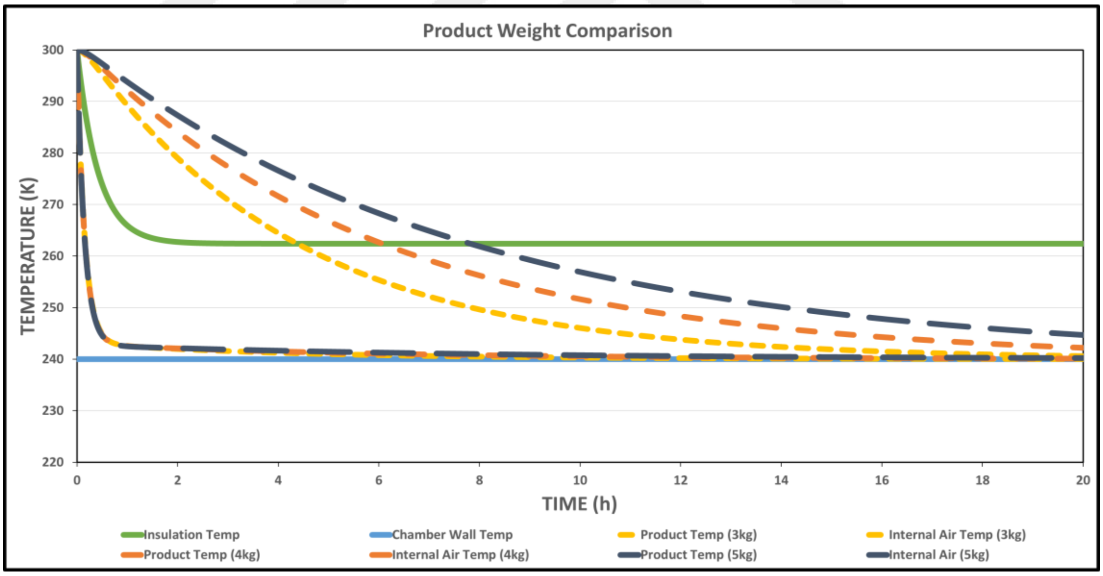

(a)

Figure 2.7 Single-step working logic temperature comparison (a), last one-hour temperatures (b)

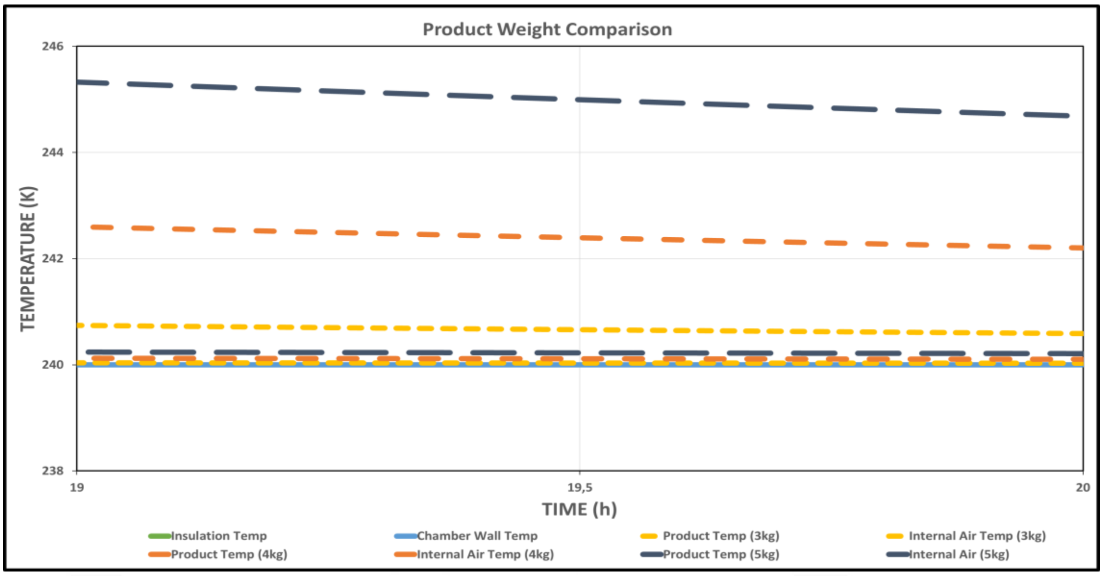

(b)

Figure 2.7 Continues

2.3.3 Absorbed Heat Comparison

The absorbed heat is solved by Eqs. (2.10)-(2.12). Product weight assumed as 5kg. First, values are high because of big temperature differences. Also similarly, there are fluctuations in gradual working logic caused by temperature changes. But apart from that absorbed heat are similar for gradual and single-step working logic.

$$Q_{absorbed_{product}}{}^{t} = m_{product} c_{p_{product}} \left(T_{product}{}^{t+1} - T_{product}{}^{t}\right) \tag{2.10}$$

$$Q_{absorbed_{intair}}{}^{t} = m_{intair} c_{p_{intair}} (T_{intair}{}^{t+1} - T_{intair}{}^{t}) \tag{2.11}$$

$$Q_{absorbed_{pu}}{}^{t} = m_{pu} c_{p_{pu}} (T_{pu}{}^{t+1} - T_{pu}{}^{t}) \tag{2.12}$$

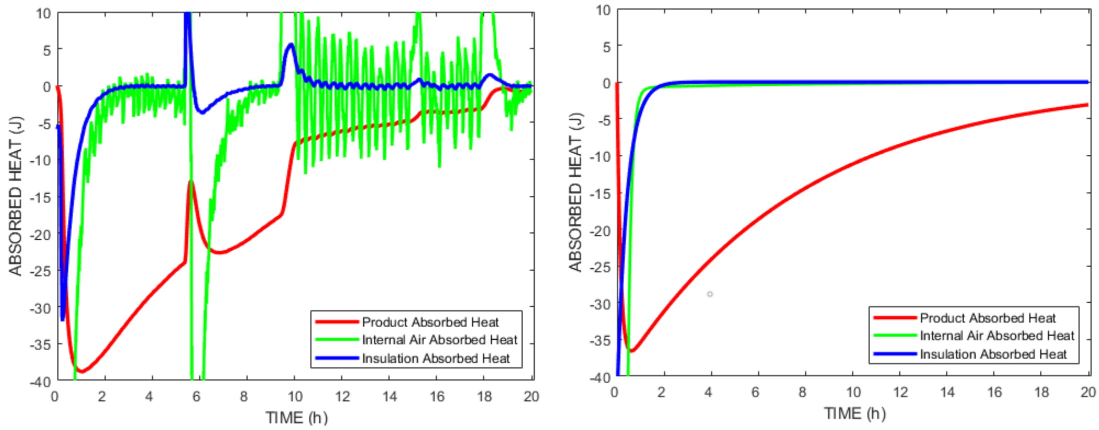

(a) (b)

Figure 2.8 Absorbed heat of gradual (a) and single-step (b) working logic

2.3.4 Evaporator Capacity Comparison

The left side is connected to internal air and the right side is connected to the insulation part. Evaporator capacity is calculated by Eqs (2.12)-(2.13). Total evaporator capacity is the sum of left and right sides. Latent heat is neglected.

$$\dot{Q}_{evapcap_{left}}{}^{t} = \frac{T_{intair}{}^{t} - T_{chmwall}{}^{t}}{R_{intair_2} + R_{chmwall} + R_{shelves}} \tag{2.12}$$

$$\dot{Q}_{evapcap_{right}}{}^{t} = \frac{T_{pu}{}^{t} - T_{chmwall}{}^{t}}{R_{pu_1}} \tag{2.13}$$

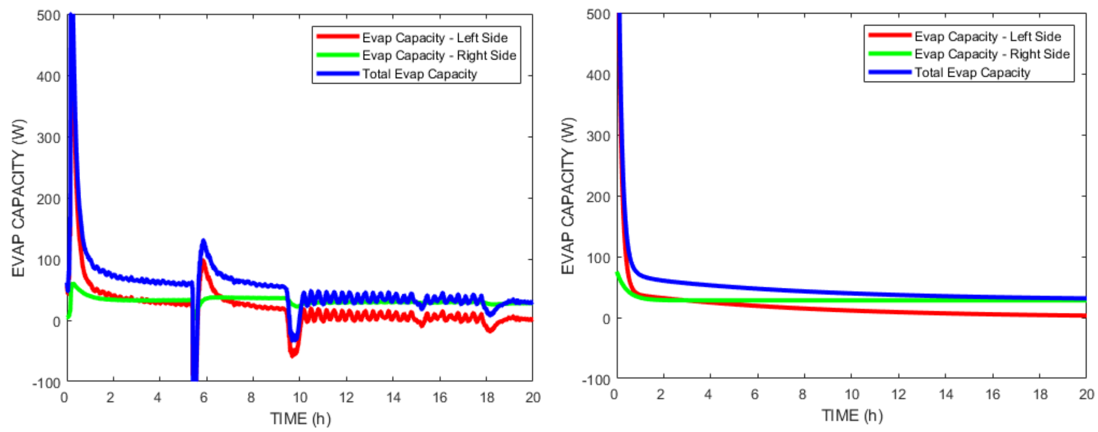

(a) (b)

Figure 2.9 Evaporator capacity of gradual (a) and single-step (b) working logic

CHAPTER THREE
PROPOSAL DESIGN OF VACUUM CHAMBER

3.1 New Chamber Design Description

Most the vacuum freezer has a cylindrical chamber containing insulation, a wrapped evaporator, compressor, and condenser. The most important reason for the cylindrical chamber is a uniform vacuum and cooling performance but the disadvantage is humidity after the drying process. After humidity removal from the product high humidity air turns back to a vacuum pump and it decreases the life cycle of the vacuum pump. In order to save the life cycle of the vacuum pump, a new design has a fin on tube evaporator inside the chamber. The major reason is the eliminate the humidity after drying and send dried air to the vacuum pump. Another benefit is to help the cooling process. Another major design change is the rectangular chamber and the reason is better placement of fin on tube evaporator. New proposal design is shown in Fig 3.1. This design is a just proposal design to understand the pros and cons of cylindrical and rectangular chambers.

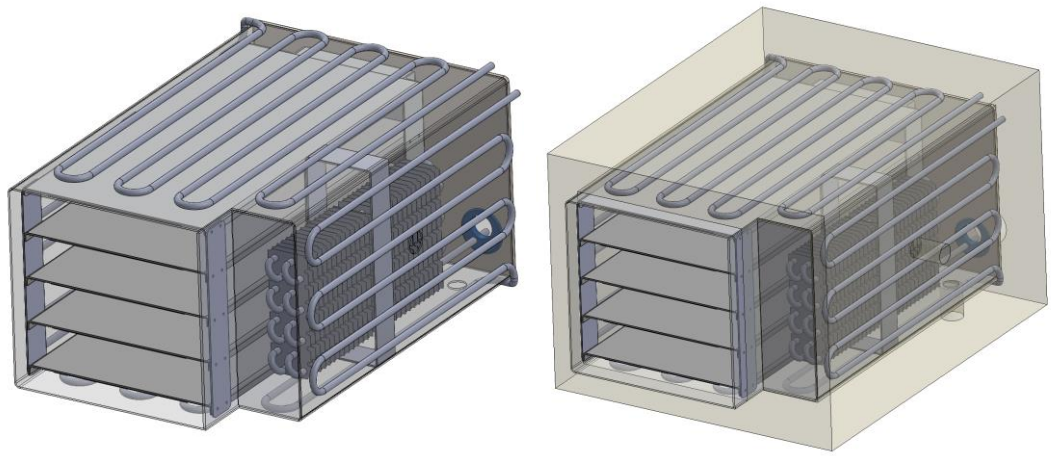

(a) (b)

Figure 3.3 The proposal design of rectangular chamber with (a) and without (b) insulation

3.2 Mechanical Analysis of Cylindrical and Rectangular Chambers

These analyses aim to see the mechanical strengths of cylindrical and rectangular chambers. Chamber inner pressure reduces after the vacuum pump starts and it creates a big pressure difference between the chamber outside and inside. This process repeats constantly for that reason, we need to run a statical analysis to check displacements of chamber surfaces. These analyses were done in Ansys v19.2

The cylindrical and rectangular chamber performed a static structural analysis. cylindrical chamber thickness is 3mm and the material is stainless steel. Firstly, rectangular chamber thickness was taken at 2mm but the fin on tube evaporator lateral wall displacement was high, for that reason there were some additional improvements to decrease displacements such as supporting frames and increase the thickness. Weight increase due to The analysis setup is shown in Fig 3.2 and 3.3. Supporting frames are shown in Fig. 3.4. The final results weight and displacement results are shown in Table 3.1.

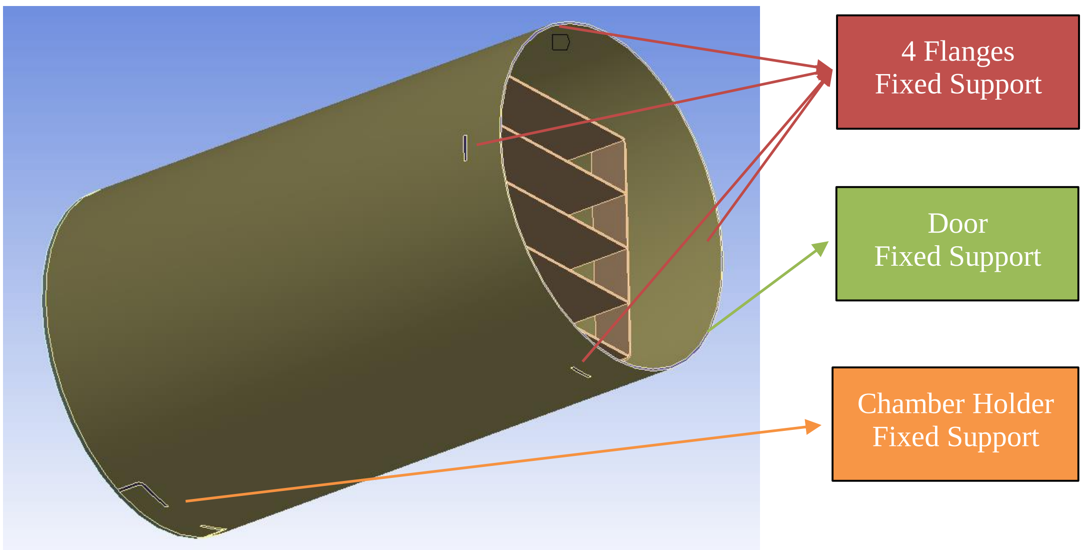

Figure 3.2 Static structural mechanical analysis setup of the cylindrical chamber

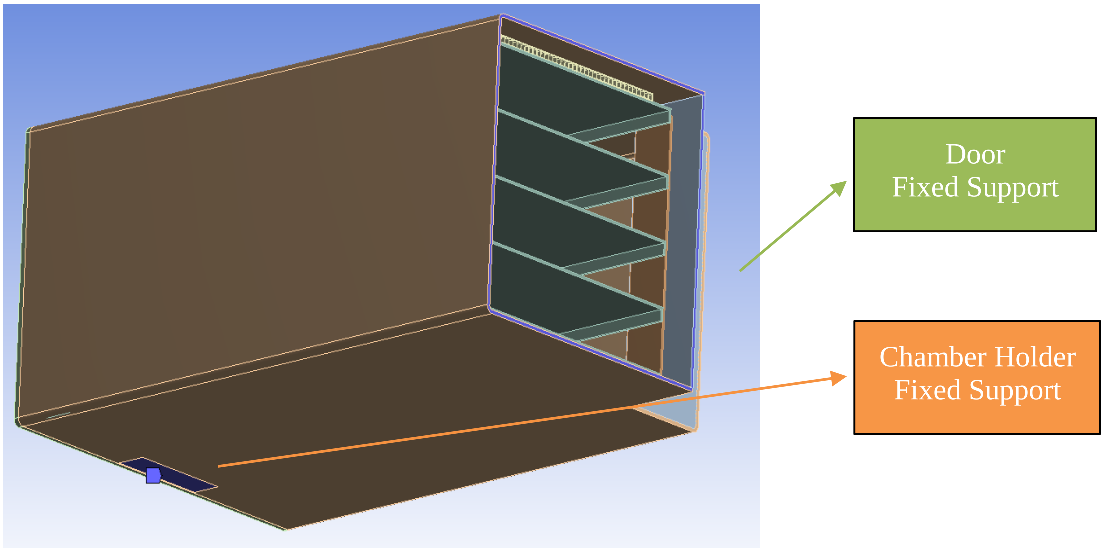

Figure 3.3 Static structural mechanical analysis setup of the rectangular chamber

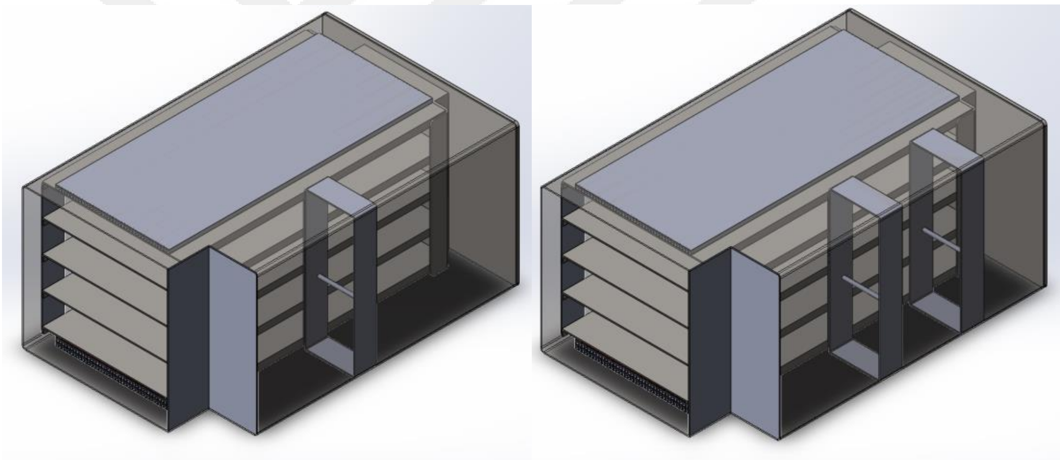

(a) (b)

Figure 3.4 Additional improvements one (a) and two (b) supporting frames

In the proposal design, the chamber holder was extended to decrease displacement on the back wall. In order to simulate pressure difference, 1 atm pressure was applied to lateral and outer surfaces which are not fixed supports.

Table 3.1 Total deformation on lateral walls of cylindrical and rectangular chamber

Design	Lateral (mm)		Back (mm)		Weight (kg)
2mm – Cylindrical	0.3		1.2		11.37
Design	**Top (mm)**	**Bottom (mm)**	**Right (mm)**	**Left (mm)**	**Weight (kg)**
3mm - rectangular with one support	0.3	0.1	1.2	0.8	17.2
2mm - rectangular with one support	0.3	0.2	3.6	1.5	12.5
3mm - rectangular with two support	0.3	0.1	0.6	0.5	17.2
2mm - rectangular with two support	0.3	0.2	1.2	1	12.5

The stainless steel material properties were taken from Ansys Workbench 19.2 library. The economic impact is the weight of the chamber and the 2mm rectangular chamber is competitive with respect to the cylindrical chamber. The right lateral wall is the most affected surface cause the fin on tube evaporator was placed there, in that case supporting frames helped to decrease the displacement. In the end, the proposed design was taken 2mm rectangular chamber with two supporting frames.

3.3 Machine Compartment Air Flow Simulation

The main parts of the vacuum freezer system are the compressor, fan condenser, and evaporator. The chamber should be isolated from hot air that comes from the condenser and compressor otherwise it will penalize cooling performance. In order to remove hot air front air grill, side air holes, and rear air grill were added to the proposal design. These are shown in Fig. 3.5. Front air grills were added for fresh air entrance, and side air holes and rear air grill were added for hot air removal purposes. Distances from walls are also important, distances from front, back, and sides are 200mm, 50mm, and 50 mm, respectively. There is a 1.5° angle which helps remove water after the drying process.

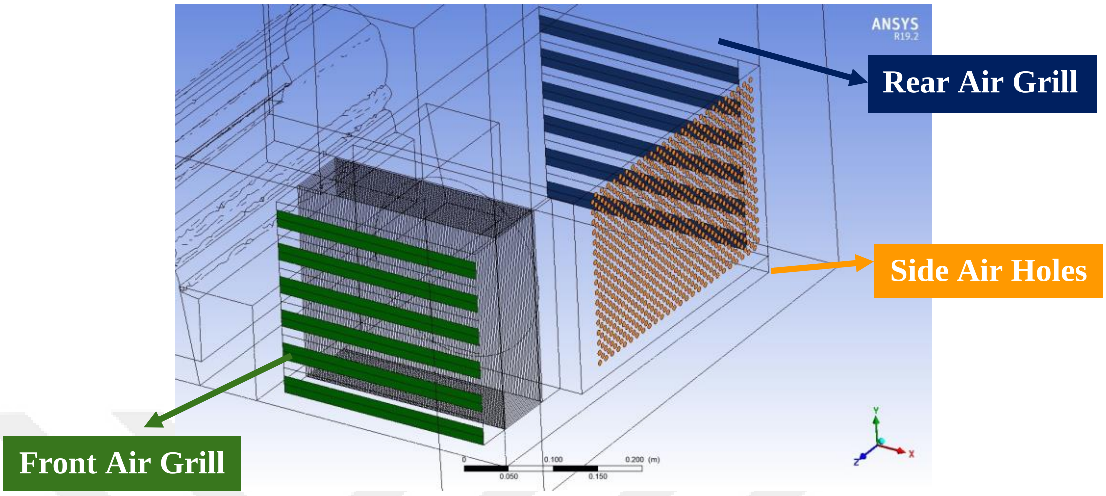

Figure 3.5 Air inlet and outlet sources

As a second step, diffuser and separator plates were added to the compressor and fan condenser compartment to isolate hot air sources from the chamber. There were two sections of isolation. First, the diffuser was placed between the front air grill and condenser, second separators were placed around the compressor and fan condenser compartment. Separators placement are shown in Fig 3.6

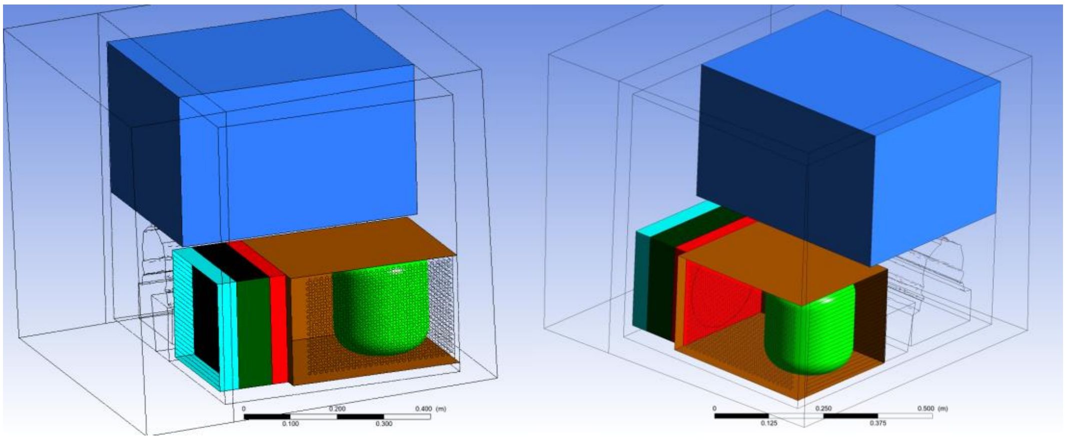

Figure 3.6 Separator and diffuser placement

The blue part is the chamber with insulation, the light blue part is the diffuser, the green part is the condenser, the red part is the fan, the green part is the compressor and the brown part is the separator. Temperatures were also observed during this CFD study and initial temperatures taken for the condenser and compressor are 353K and 323K, respectively. There was heat flux to simulate heat transfer from hot sources to the chamber, 30 W/m^2 was taken respectively. The hot air should remove from the condenser and compressor by the fan and it should not enter to machine compartment again. Mass flow rates are crucial to understanding fresh air entrance and hot air removal amount which are directly affecting the cooling performance of the system. Mass flow rates are shown in Table 3.2.

Table 3.2 Mass flow rates of grills, holes, and condenser inlet

	Design - 1 without isolation	**Design - 2 with isolation**
	Mass Flow Rate (kg/s)	
Front Air Grill	0.167	0.089
Rear Air Grill	-0.094	-0.075
Side Air Holes	-0.073	-0.014
Condenser Inlet	0.167	0.203

These results indicated that without isolation design is better in terms of mass flow rates of grills and holes but the condenser inlet was lower. Understand the real reason, airflow simulation results were processed in the FieldView CFD program. Results proved that some hot air is not able to exit from the rear grill and side holes and it recirculates between the condenser inlet and outlet which is efficiency loss and impact on cooling performance. Airflow directions are shown in Fig. 3.7 and 3.8.

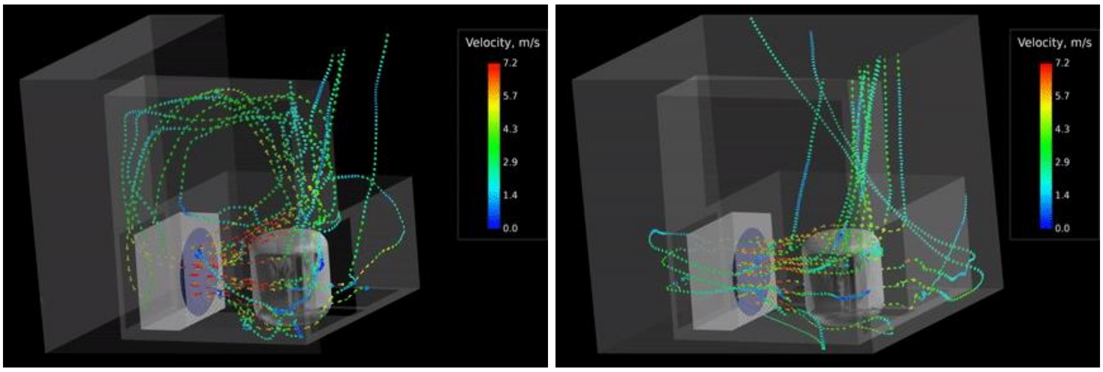

(a) (b)

Figure 3.7 Airflow without diffuser and separator (a) and with diffuser and separator (b)

The surface average temperatures of the insulation walls, diffuser, and separator. Volume average temperature of the machine compartment which is ejected with the diffuser and separator and the rest of the vacuum freezer internal air temperature are shown in Table 3.3. Volumes are shown in Fig 3.8.

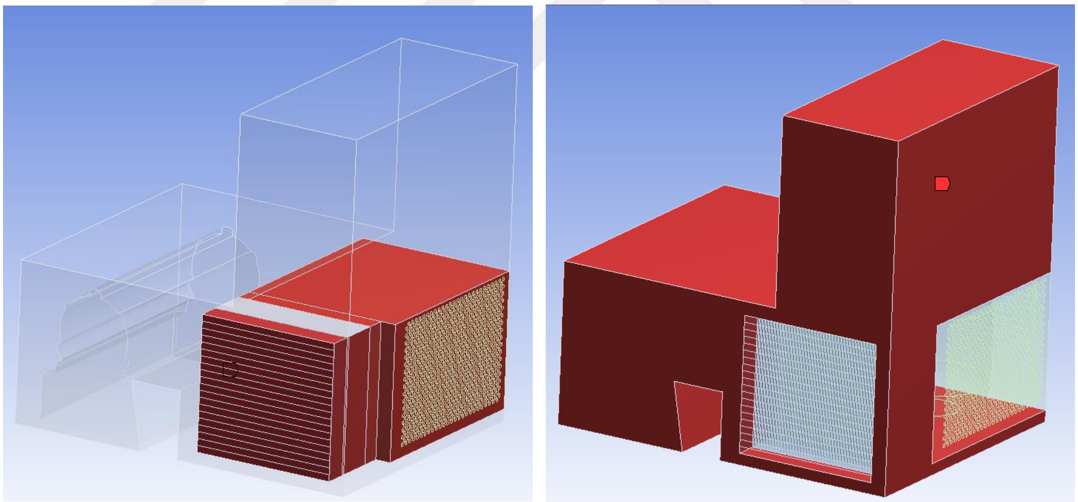

(a) (b)

Figure 3.8 Volume of machine compartment (a) and rest of internal air of vacumm freezer (b)

Table 3.2 Temperature results of selected walls

	Design - 1 without isolation	Design - 2 with isolation	Delta
	Temperatures (K)		
Chamber Top Wall	286.9	285.3	+1.6
Chamber Bottom Wall	324.0	340.5	-16.5
Chamber Right Wall	313.3	340.2	-26.9
Separator	336.3	342.7	-6.4
Diffuser	331.7	340.9	-9.2
Machine Compartment	335.0	339.6	-4.6
Rest of Internal Air	325.8	342.6	-16.8

These temperatures demonstrated that the diffuser and separator got a huge impact on isolation between cold and hot sections. A combined view of the temperature distributions of chamber top, bottom, and right walls are shown in Fig 3.9. The separated view is shown in Fig 3.10.

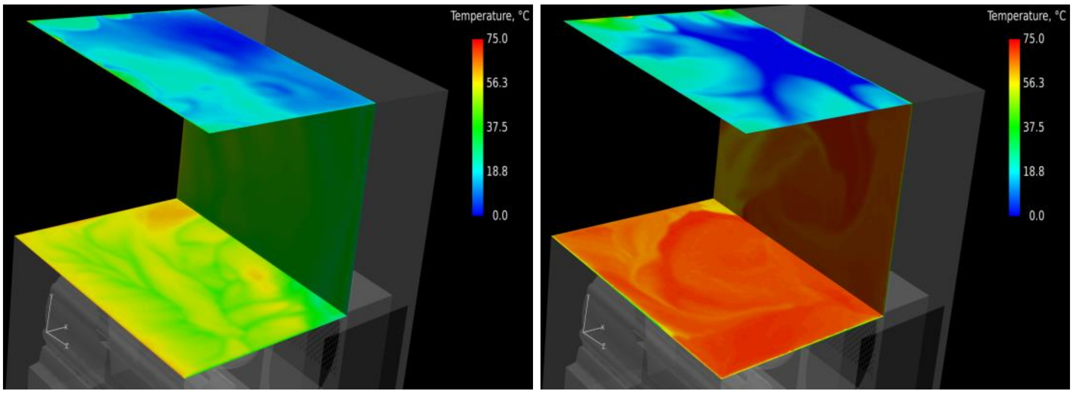

(a) (b)

Figure 3.9 Combined view of temperature distribution of the top, bottom, and right wall with isolation (a) and without isolation (b)

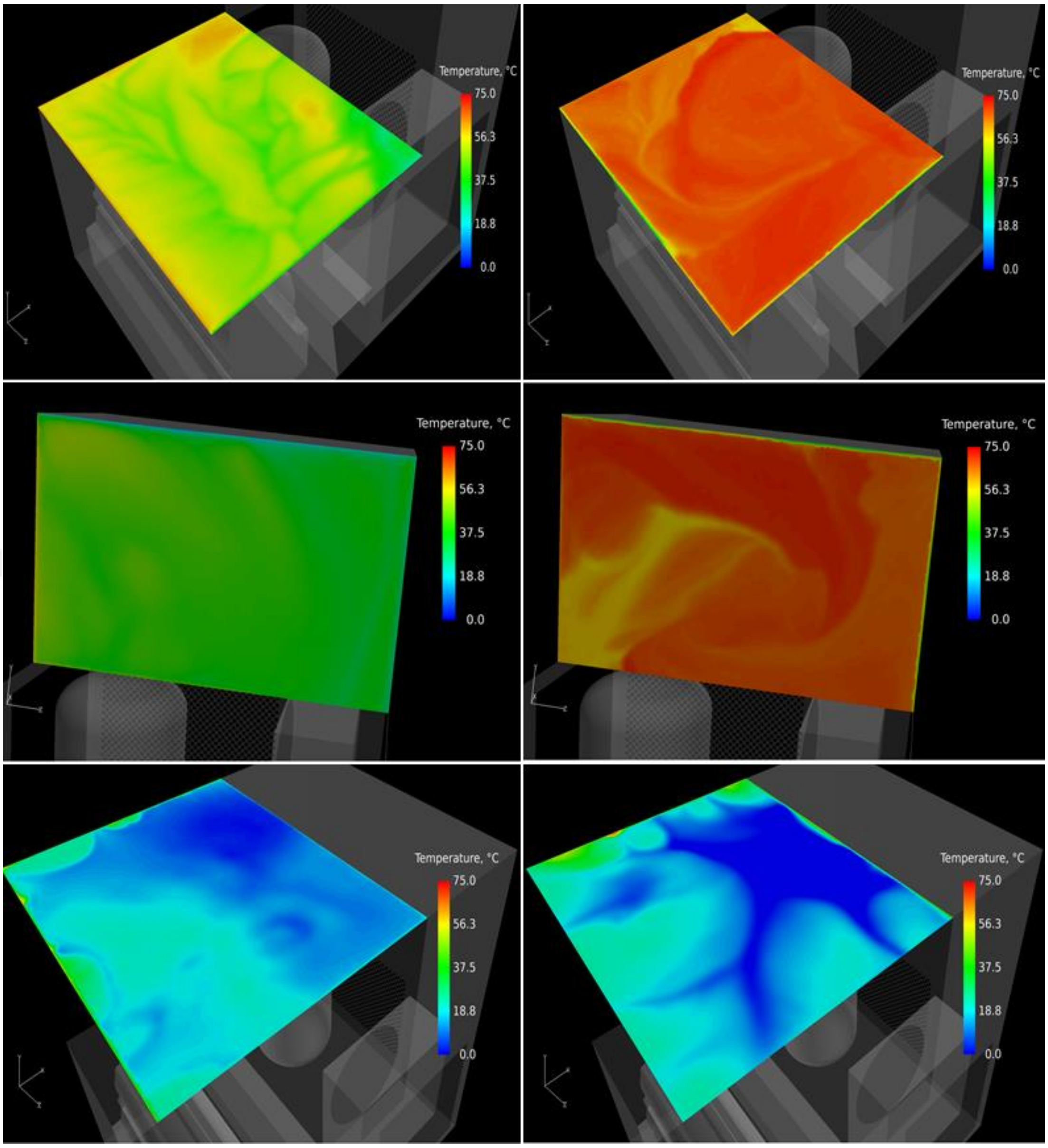

(a) (b)

Figure 3.10 Temperature distribution of bottom, right, and the top wall of the chamber with isolation (a) and without isolation (b)

These figures proved that diffuser and separator affected temperature isolation significantly but this isolation affected the mass flow rate passing through the condenser. The heat transfer rate of the condenser was investigated with Eq. (3.10).

$$\dot{Q}_{\mathrm{cond}} = \dot{m}c_p\Delta T = \dot{m}c_p(\mathrm{T}_{\mathrm{cond}_{\mathrm{outlet}}} - \mathrm{T}_{\mathrm{cond}_{\mathrm{inlet}}}) \tag{3.10}$$

The heat transfer rates with diffuser and separator and without them were 4132W and 3200W. The mass flow rate was higher without a diffuser and separator but the inlet and outlet temperature of the condenser were higher. It boosted the condenser heat transfer by %29.

The conclusion of these analyses was diffuser and separator usage increase cooling performance plus boost cooling speed, energy consumption, and noise level of vacuum freezer. Flow analysis setup assumed as the vacuum freezer in the kitchen and back wall distance was 50mm which affected the hot air removal from the vacuum freezer significantly. For that reason, this distance should be considered from the customer's perspective.

3.4 Steady-State Thermal Analysis of Cooling Volume

The aim of this analysis was the insulation around the chamber which impacts directly to cooling speed and refrigeration performance of the system. Cooling volume is shown in Fig 3.11 and mesh details are shown in Fig 3.12. Assumptions are;

- Insulation thermophysical properties were taken the same as in Chapter 2,
- Evaporator pipes were neglected,
- Contact surfaces between evaporator and chamber were accepted as evaporator surfaces,
- 40mm, 45mm, and 50mm insulation thicknesses were studied with 245K and 255K evaporator temperatures.

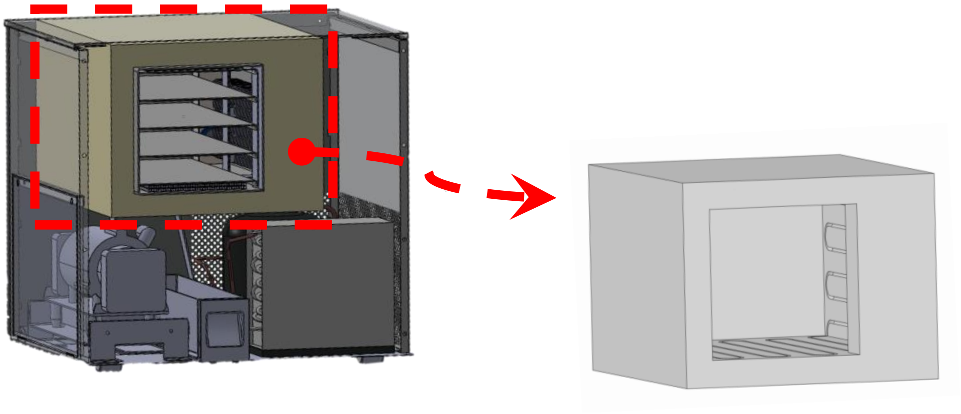

Figure 3.11 Cooling volume for steady-state CFD analysis

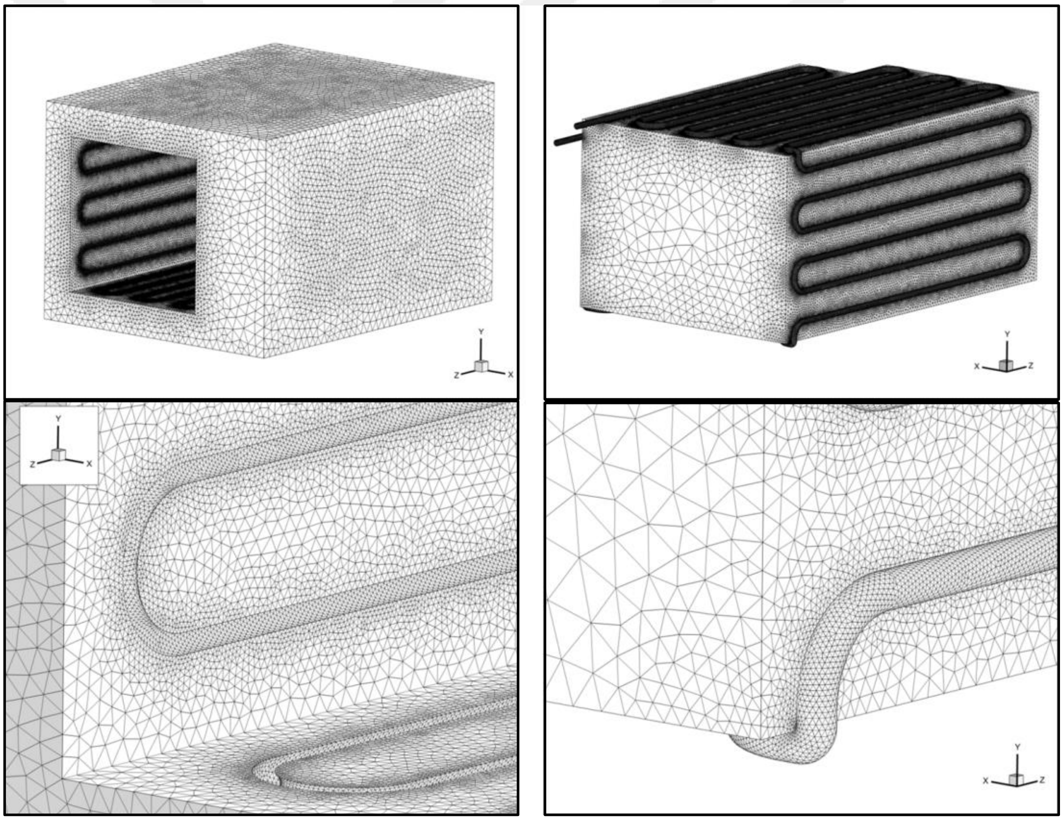

Figure 3.12 Mesh details of CFD model

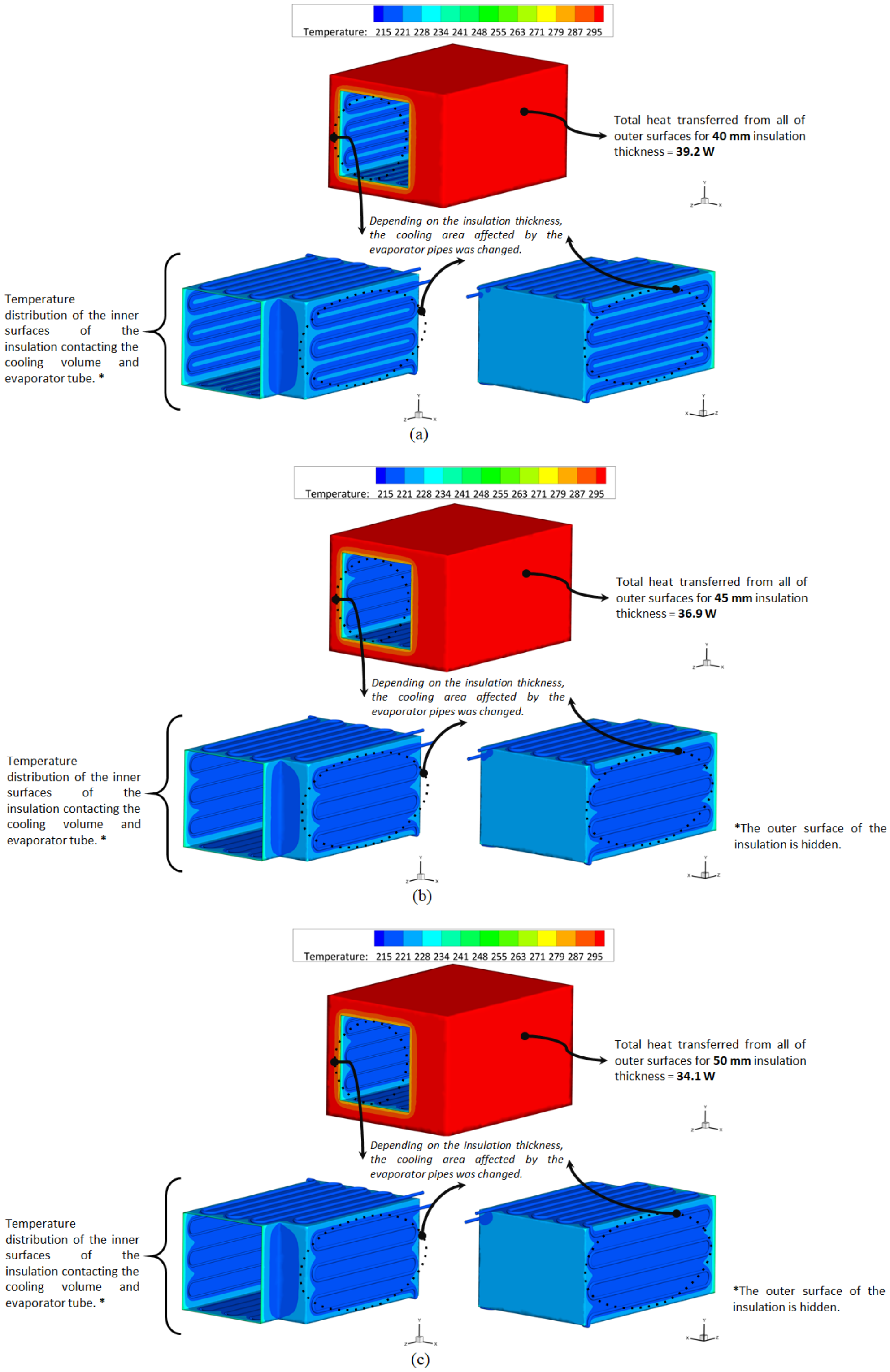

Figure 3.13 Temperature distribution of 255K evaporator temperature with 40mm (a), 45mm (b), and 50mm (c) insulation thickness

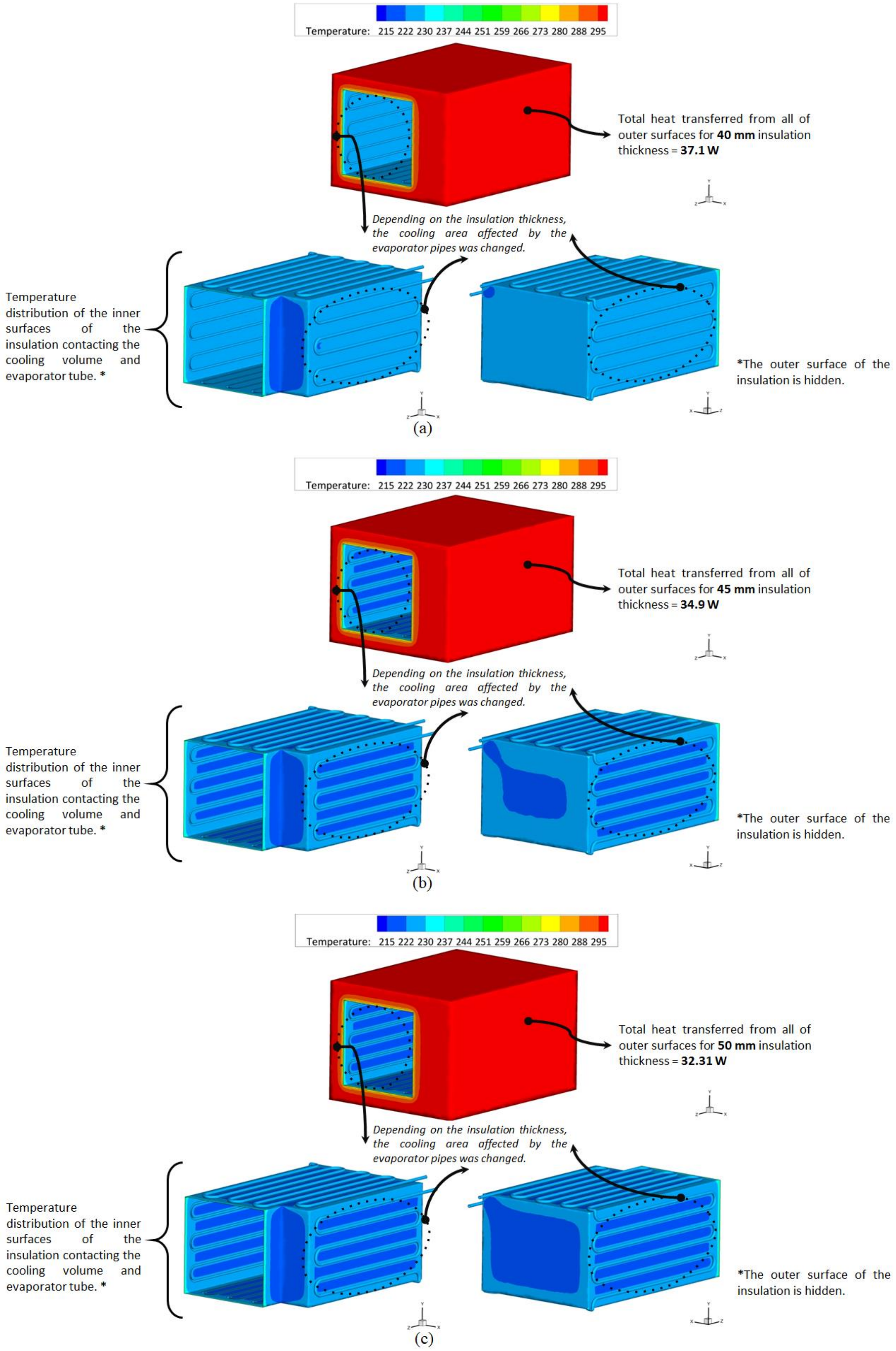

Figure 3.14 Temperature distribution of 245K evaporator temperature with 40mm (a), 45mm (b), and 50mm (c) insulation thicknesses

Table 3.3 Heat gain results for different evaporator temperatures and insulation thicknesses

	Insulation 40mm	Insulation 45mm	Insulation 50mm
	Heat Gain (W)		
245K	37.1	34.9	32.3
255K	39.2	36.9	34.1

The analyses results are shown in Fig 3.13 and Fig 3.14. Heat gain differences are approximately %6 between 40mm and 45mm, %8 between 45mm and 50mm. The insulation thickness impacts the overall dimension of the vacuum freezer for that reason average thickness, 45mm, was selected as the final thickness.

3.5 Transient Thermal Analysis of Cooling Volume

The aim of this study, determine the energy amount for the cooling process and simulate it transiently. Insulation thickness was chosen according to the previous study, steady-state thermal analysis. Differently, the fin on tube evaporator was added to the cooling volume to understand the effect on cooling performance. The vacuum freezer has a plexiglass door which is considered in this analysis. Additionally, chamber thickness increased to 6mm in order to consult the thermal resistances of shelves and supporting frames. Cooling volume for transient analysis is shown in Fig 3.15 and mesh details are shown in Fig 3.16. Preliminary design experimental test result is shown in Fig 3.17. Assumptions for the transient analysis are;

- Evaporators were neglected similar to steady-state analysis and contact surfaces were considered.
- The thermophysical properties were taken the same as Chapter 3.4.

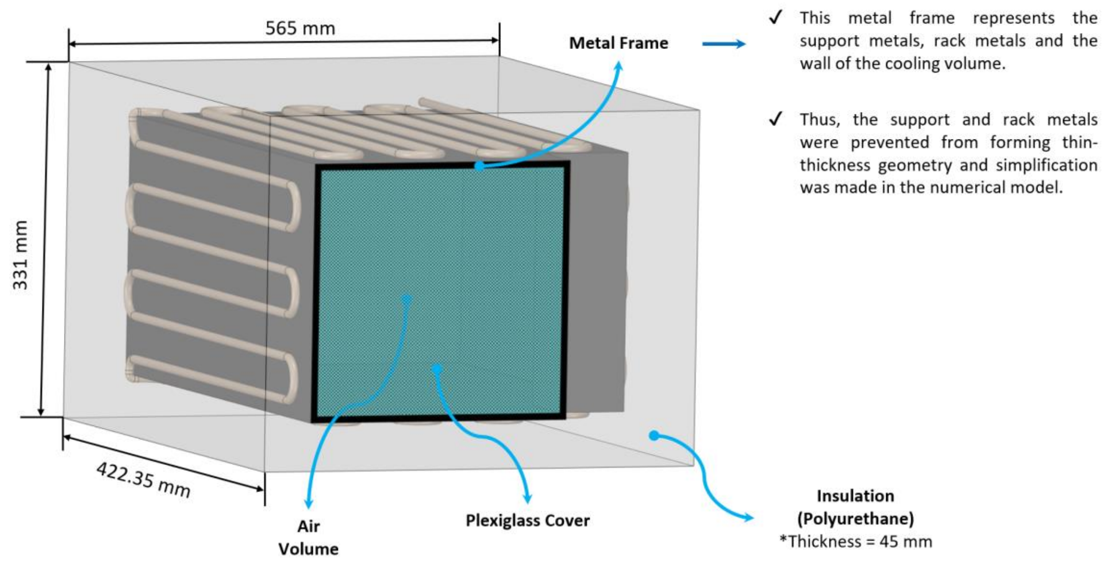

Figure 3.15 Cooling volume for transient CFD analysis

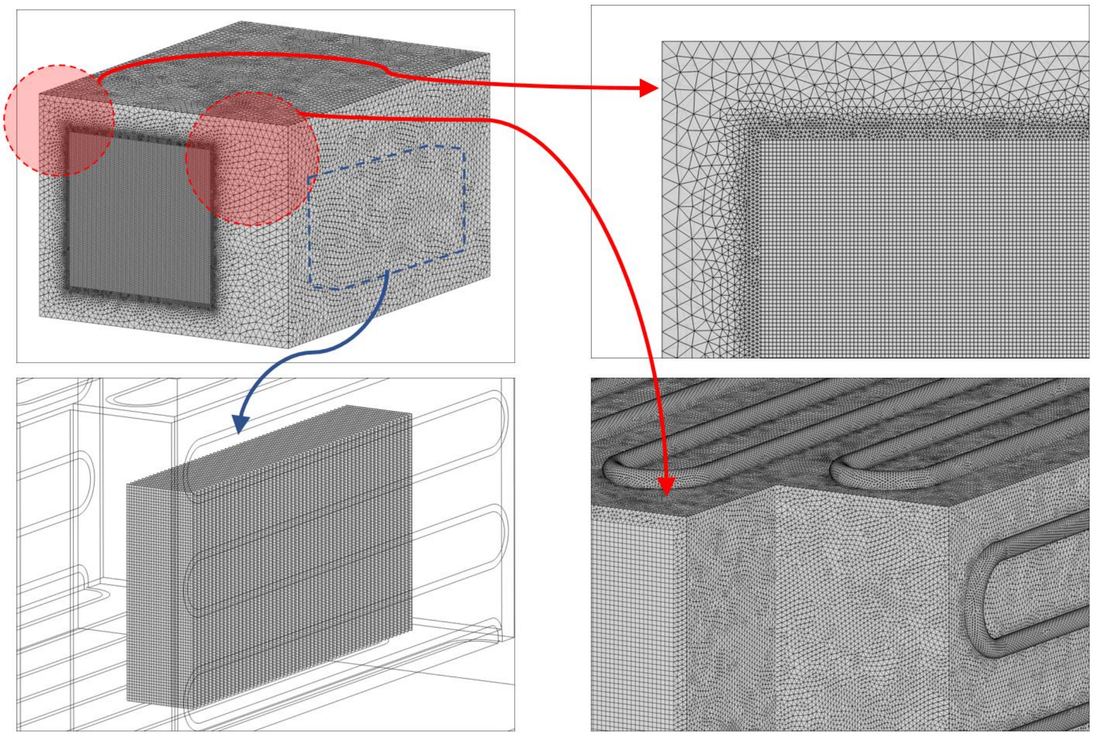

(a)

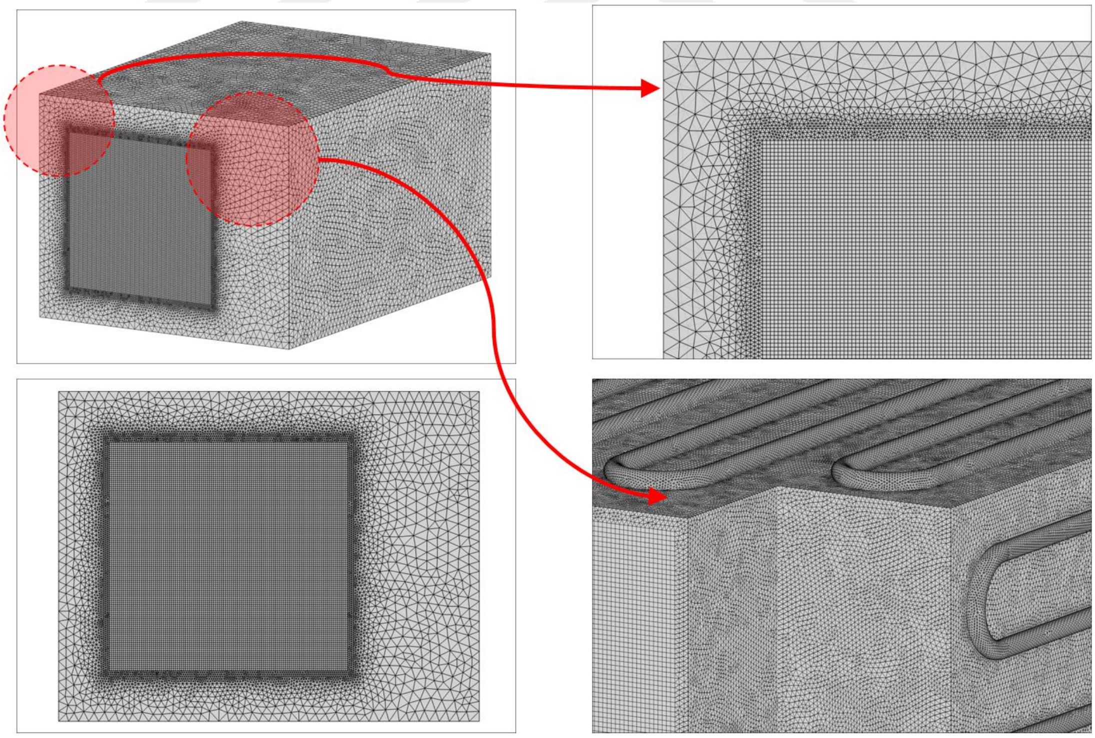

(b)

Figure 3.16 With (a) and without (b) the fin on tube evaporator CFD model for transient thermal analysis

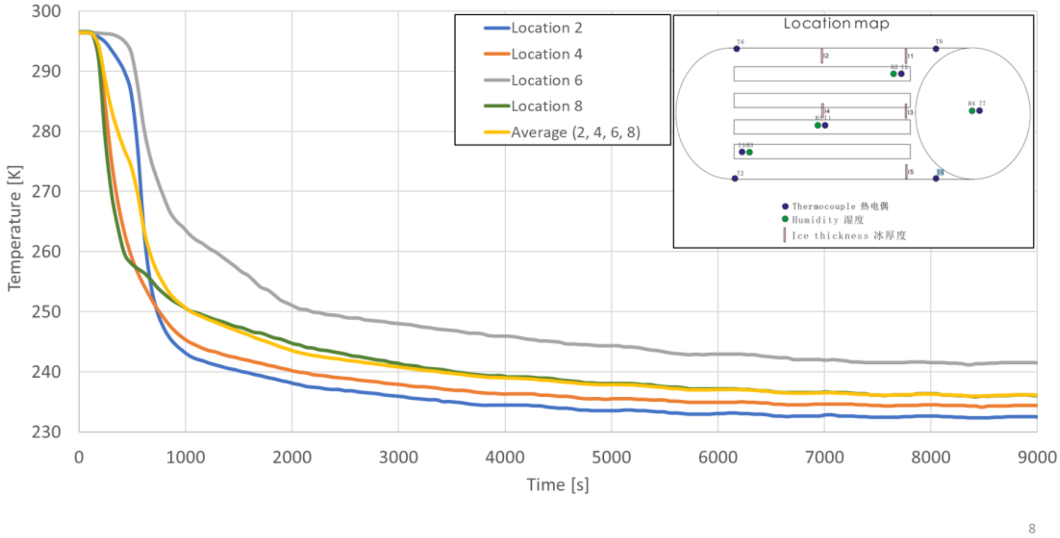

Figure 3.17 Experimental test temperature results

3.5.1 T_{evap}=228K and Without Fin on Tube Evaporator

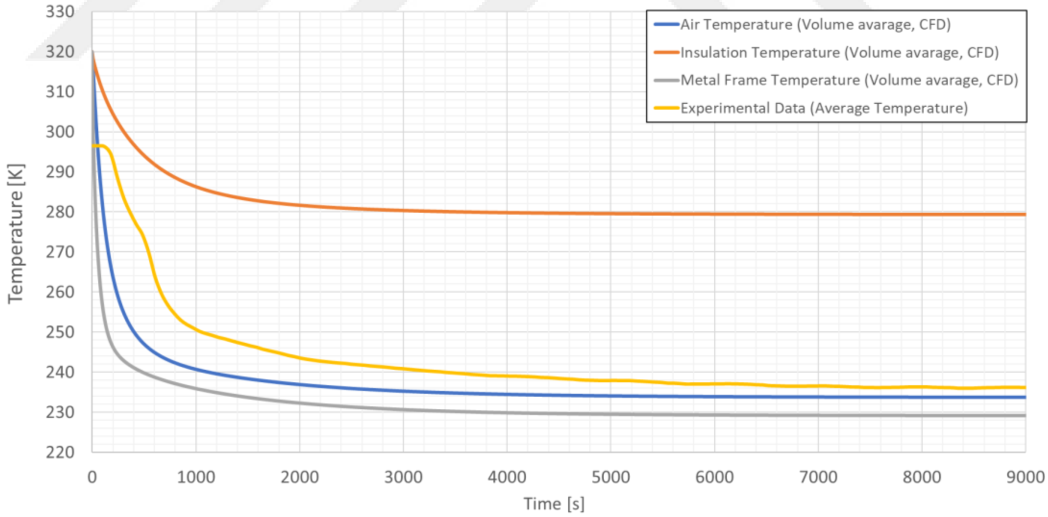

Figure 3.18 Temperature comparison between CFD and experimental results

Air, insulation, and metal frame temperatures were examined with the CFD method, and results were compared with experimental results.

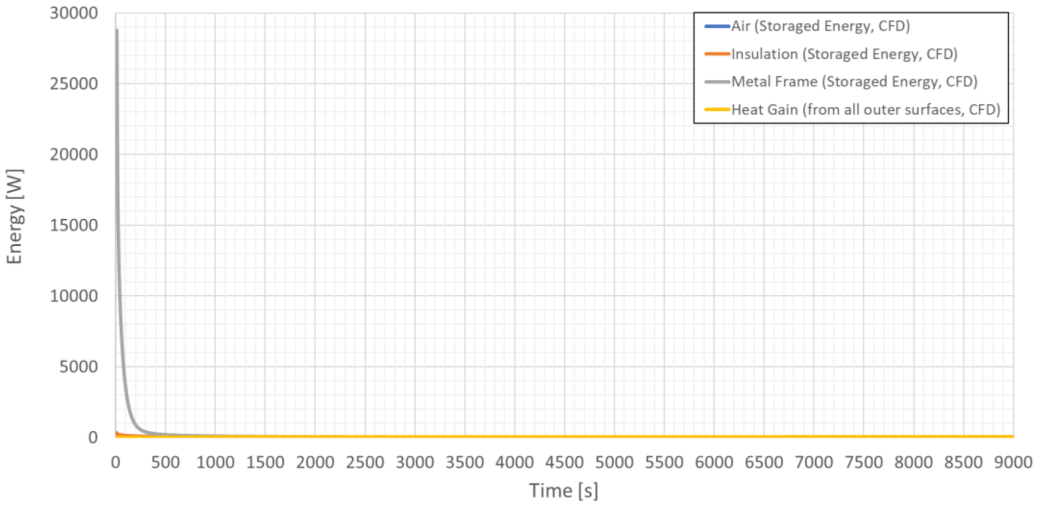

Figure 3.19 Heat gain and energy storages of air, insulation and metal frame

Energy storage is shown in Fig 3.19. Initially, the highest energy storage was seen in the metal volume due to its high thermal conductivity. In order to examine the energy storage of air and insulation zones, a closer view is shown in Fig 3.20.

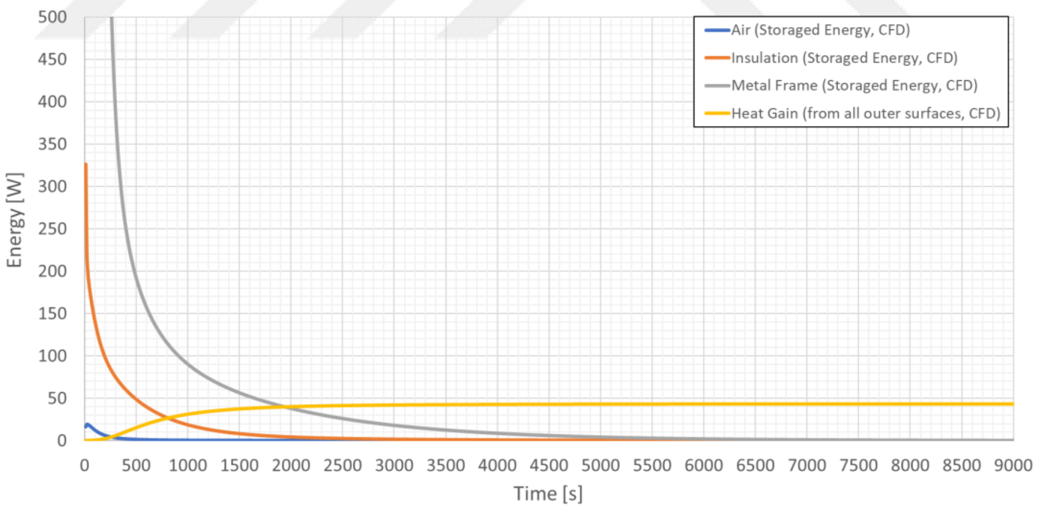

Figure 3.20 Closer view to air, insulation, and metal frame energy storages and heat gain

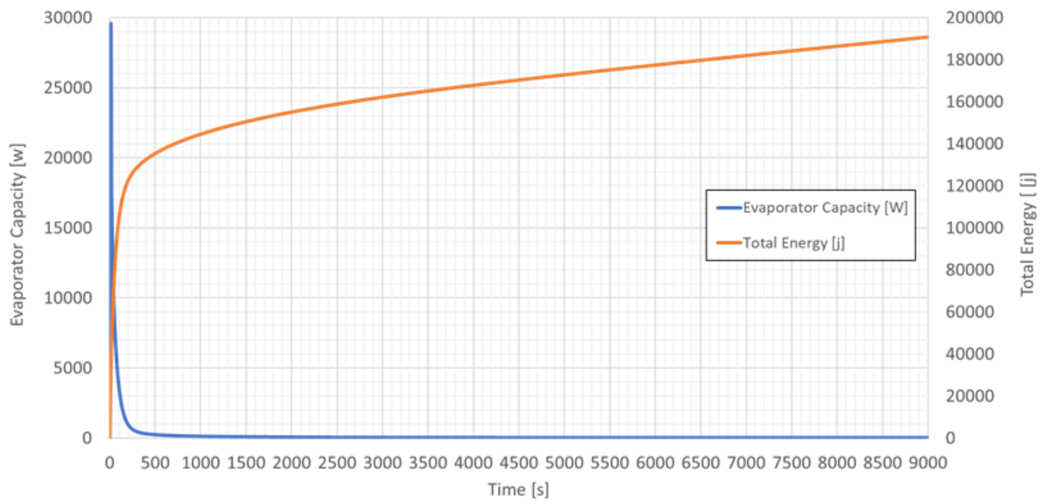

Figure 3.21 Evaporator capacity and total energy

Evaporator capacity and total energy relation are shown in Fig. 3.21. Initially, the highest energy storage was seen in the metal volume due to its high thermal conductivity. In order to examine evaporator capacity at the first 1000s, a closer view is shown in Fig 3.22.

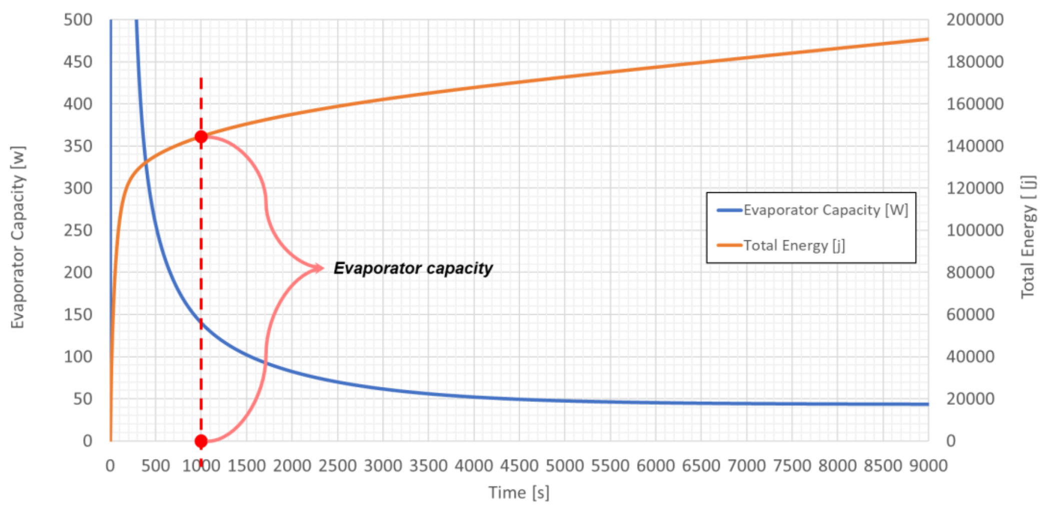

Figure 3.22 Evaporator capacity

Evaporator capacity is calculated to reduce the temperature at first 1000s which is important for starting to reduce the temperature inside the chamber.

$$\dot{Q}_{evap} = \frac{Q}{t} = \frac{144588.9}{1000} = 144.59 \text{ W} \tag{3.11}$$

3.5.2 T_{evap}=228K and With Fin on Tube Evaporator

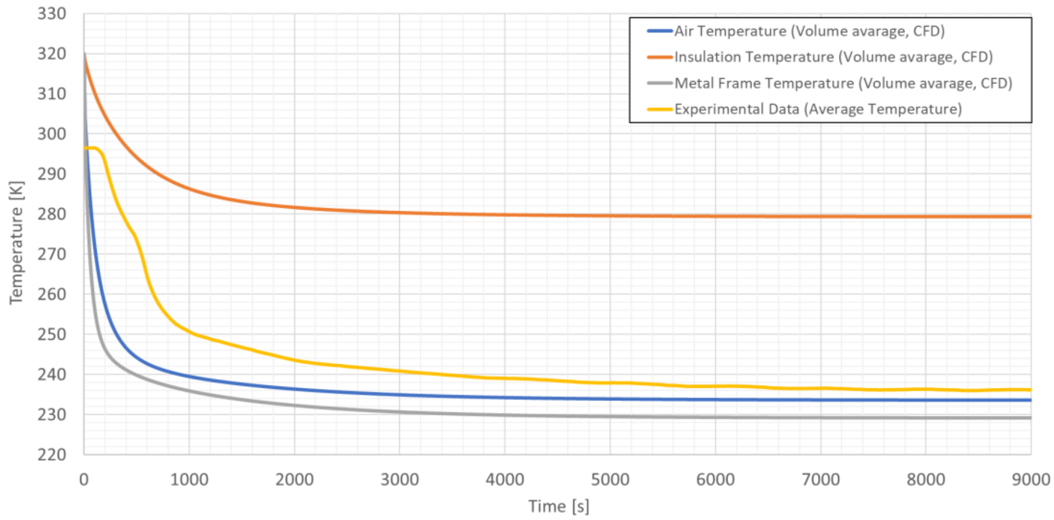

Figure 3.23 Temperature comparison between CFD and experimental results

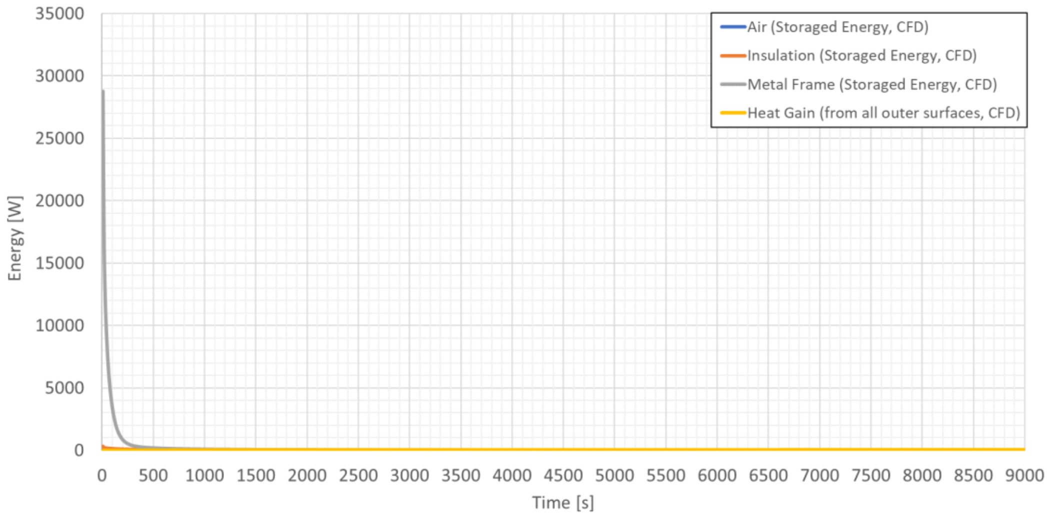

Figure 3.24 Heat gain and energy storages of air, insulation, and metal frame

Energy storage is shown in Fig 3.24. Initially, the highest energy storage was seen in the metal volume due to its high thermal conductivity. In order to examine energy storage of air and insulation zones, a closer view in the figure shown in Fig 3.25.

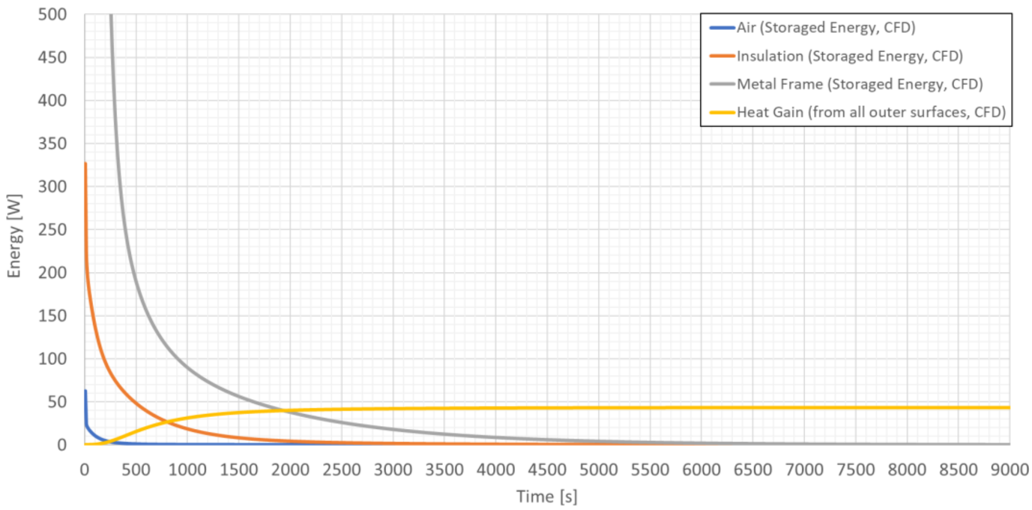

Figure 3.25 Closer view of air, insulation, metal frame energy storages and heat gain

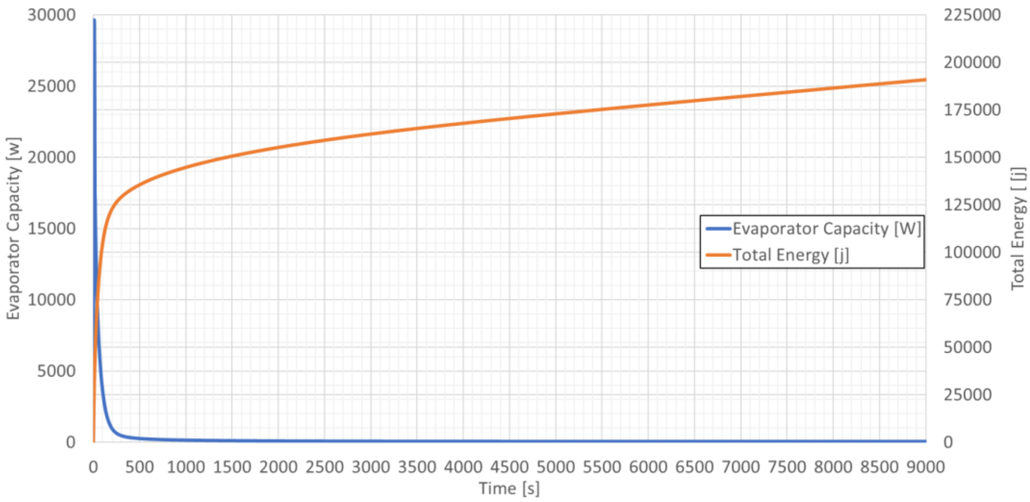

Figure 3.26 Evaporator capacity and total energy

Evaporator capacity and total energy relation are shown in Fig. 3.26. Initially, the highest energy storage was seen in the metal volume due to its high thermal conductivity. In order to examine evaporator capacity at the first 1000s, a closer view is shown in Fig 3.27.

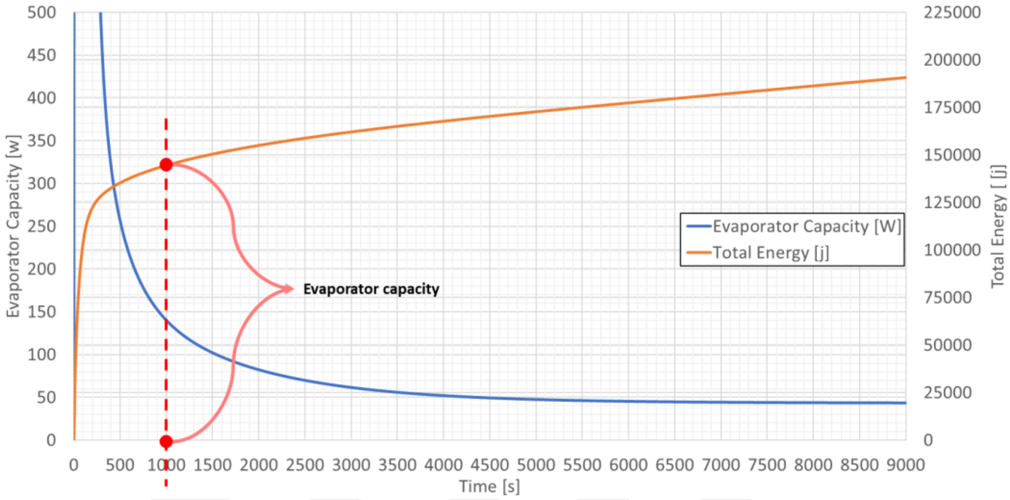

Figure 3.27 Evaporator capacity calculation

Evaporator capacity is calculated to reduce the temperature at first 1000s which is important for starting to reduce the temperature inside the chamber.

$$\dot{Q}_{evap} = \frac{Q}{t} = \frac{144611.1}{1000} = 144.6\ \mathrm{W} \tag{3.12}$$

3.5.3 T_{evap}=218K and Without Fin on Tube Evaporator

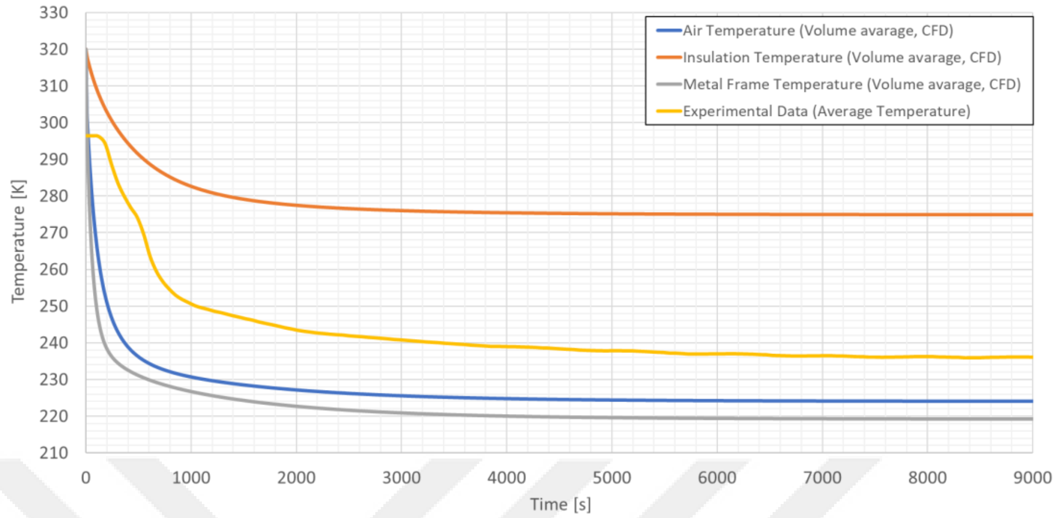

Figure 3.28 Temperature comparison between CFD and experimenteal results

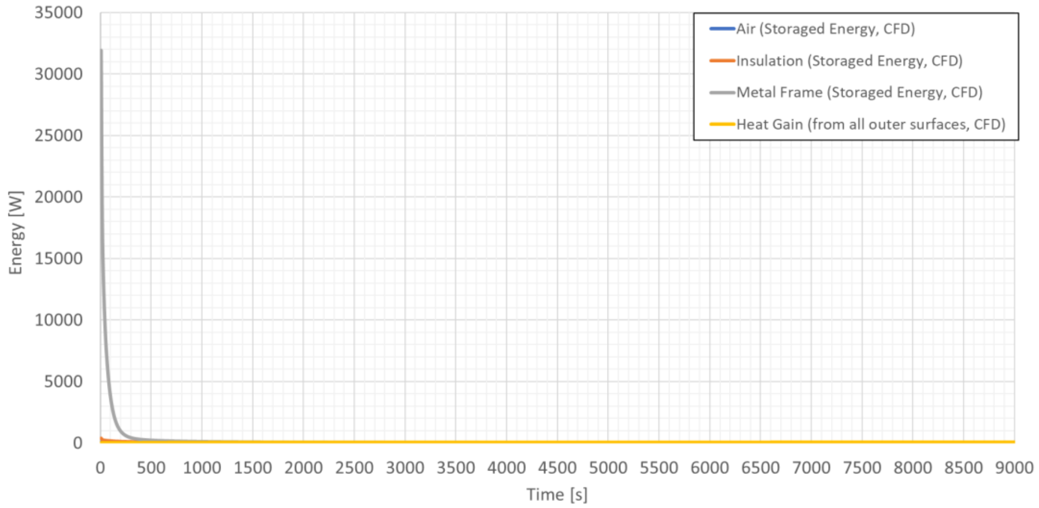

Figure 3.29 Heat gain and energy storages of air, insulation and metal frame

Energy storage is shown in Fig 3.29. Initially, the highest energy storage was seen in the metal volume due to its high thermal conductivity. In order to examine the energy storage of air and insulation zones, a closer view is shown in Fig 3.30.

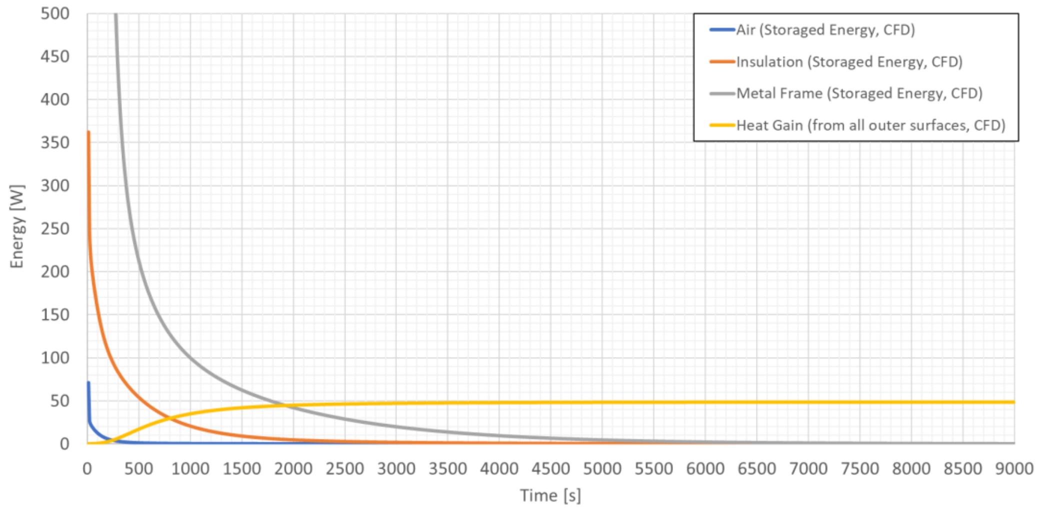

Figure 3.30 Closer view to air, insulation, and metal frame energy storages and heat gain

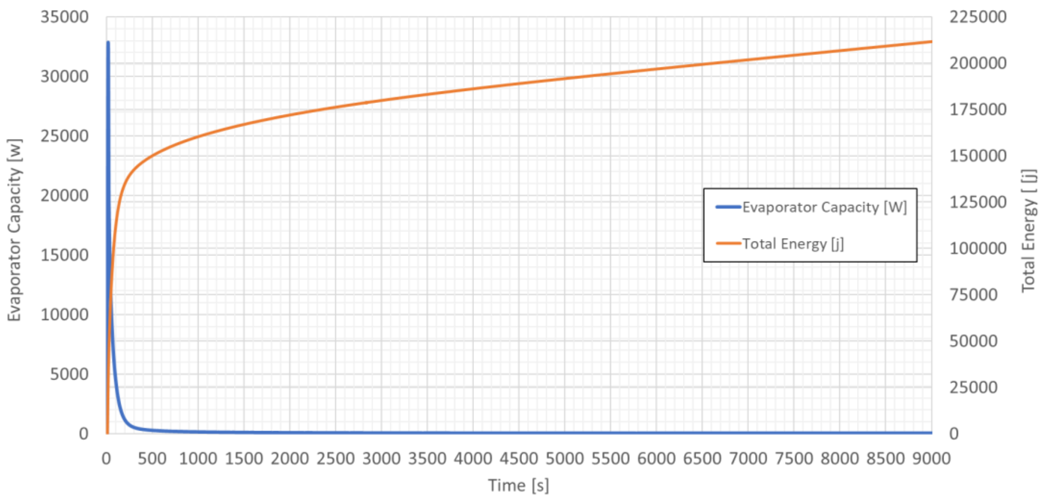

Figure 3.31 Evaporator capacity and total energy

Evaporator capacity and total energy relation are shown in Fig. 3.31. Initially, the highest energy storage was seen in the metal volume due to its high thermal conductivity. In order to examine evaporator capacity at first 1000s, a closer view is shown in Fig 3.32

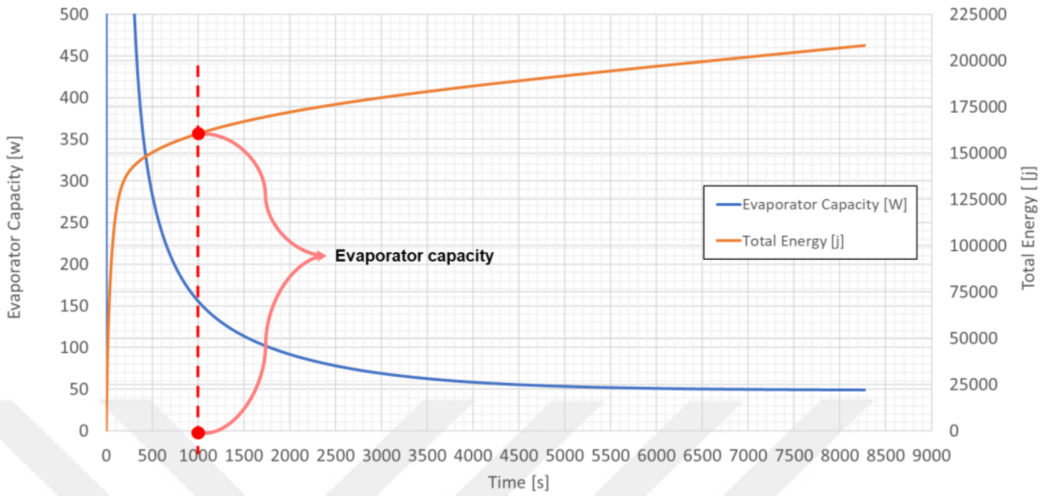

Figure 3.32 Evaporator capacity calculation

Evaporator capacity is calculated to reduce the temperature at first 1000s which is important for starting to reduce the temperature inside the chamber.

$$\dot{Q}_{evap} = \frac{Q}{t} = \frac{160359.9}{1000} = 160.36\ W \quad (3.13)$$

3.5.4 T_{evap}=218K and With Fin on Tube Evaporator

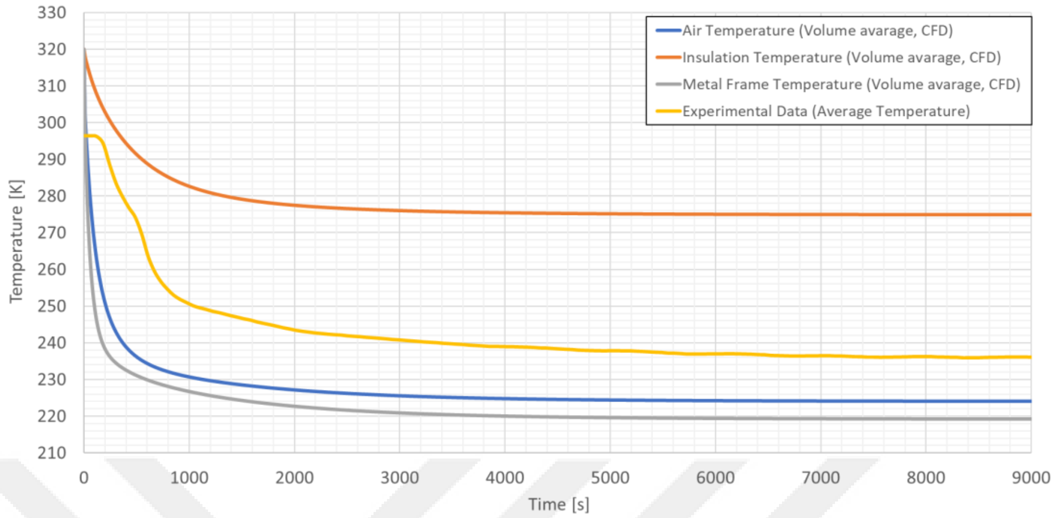

Figure 3.33 Temperature comparison between CFD and experimental results

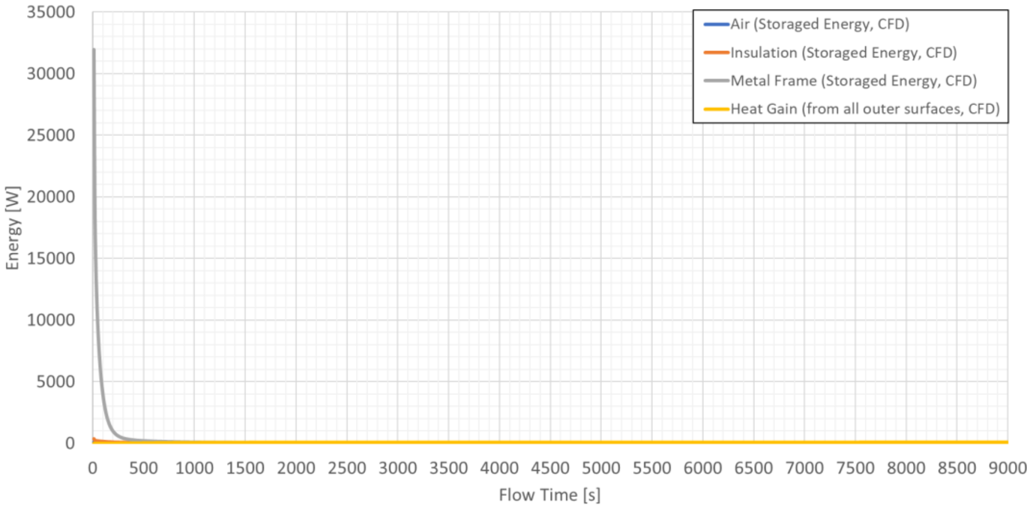

Figure 3.34 Heat gain and energy storages of air, insulation, and metal frame

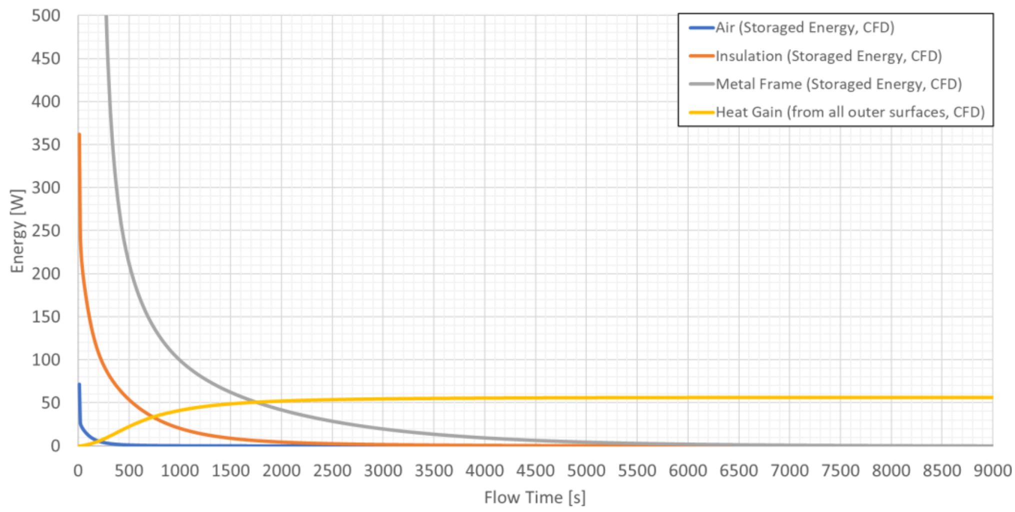

Figure 3.35 Closer view to air, insulation, and metal frame energy storages and heat gain

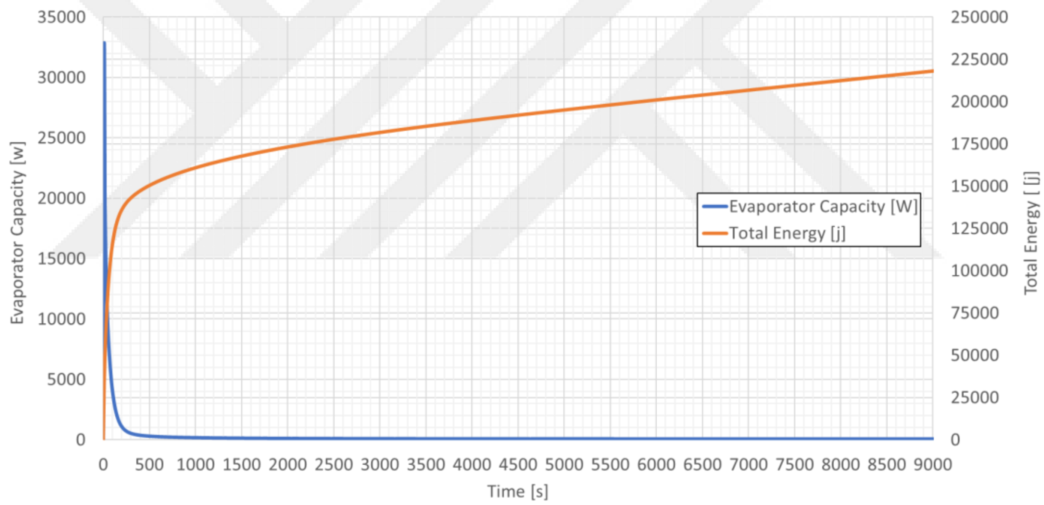

Figure 3.36 Evaporator capacity and total energy

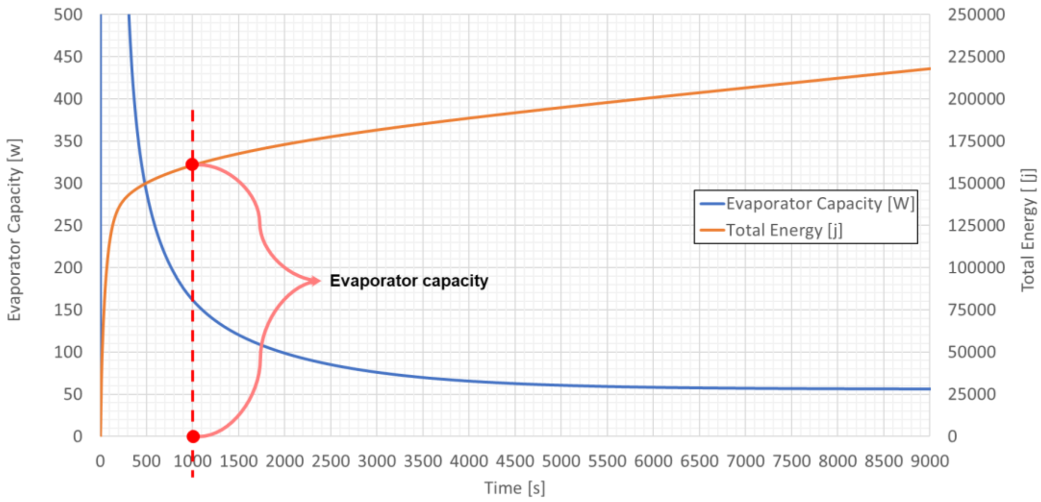

Figure 3.37 Evaporator capacity calculation

Evaporator capacity was calculated to reduce the temperature at first 1000s which is important for starting to reduce the temperature inside the chamber.

$$\dot{Q}_{evap} = \frac{Q}{t} = \frac{160814.6}{100} = 160.8\ \mathrm{W} \tag{3.4}$$

In this case, also we have calculated evaporator capacity in Chapter 2 by the TECM method for cylindrical chamber and evaporator capacity was chosen150W for safer and better cooling performance. In this section, new evaporator pipes with and without fin on tube evaporator designs proved that evaporator capacities were similar for both designs. It means one-dimensional analysis results and 3D CFD results were aligned.

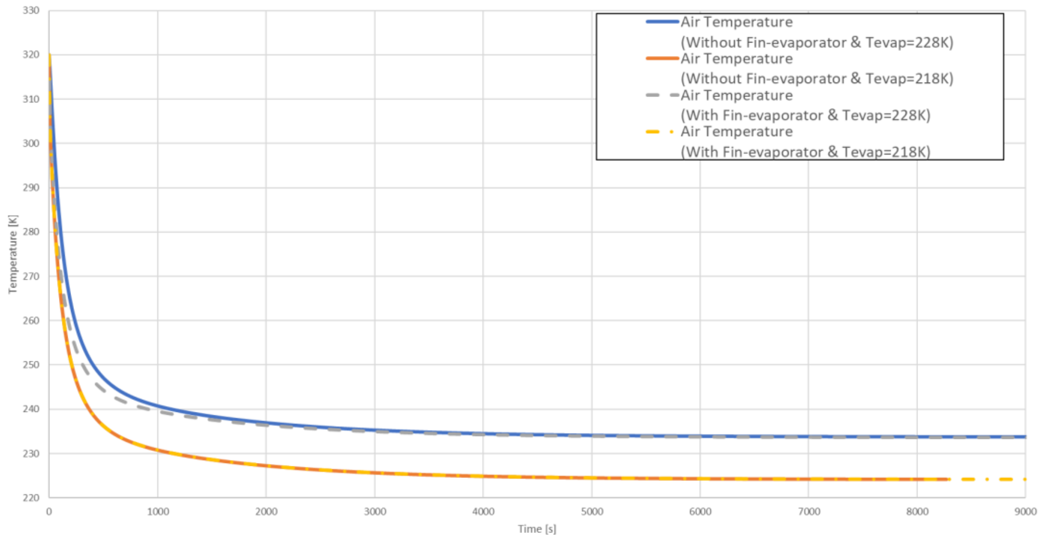

Figure 3.38 Overall air temperatures of 218K and 228K with and without fin on tube evaporator

Air temperature has a major effect on the products and 218K and 228K cooling temperatures were analyzed with and without fin on tube evaporator in Fig 3.38. Results show that the fin on tube evaporator has a good effect on the cooling rate.

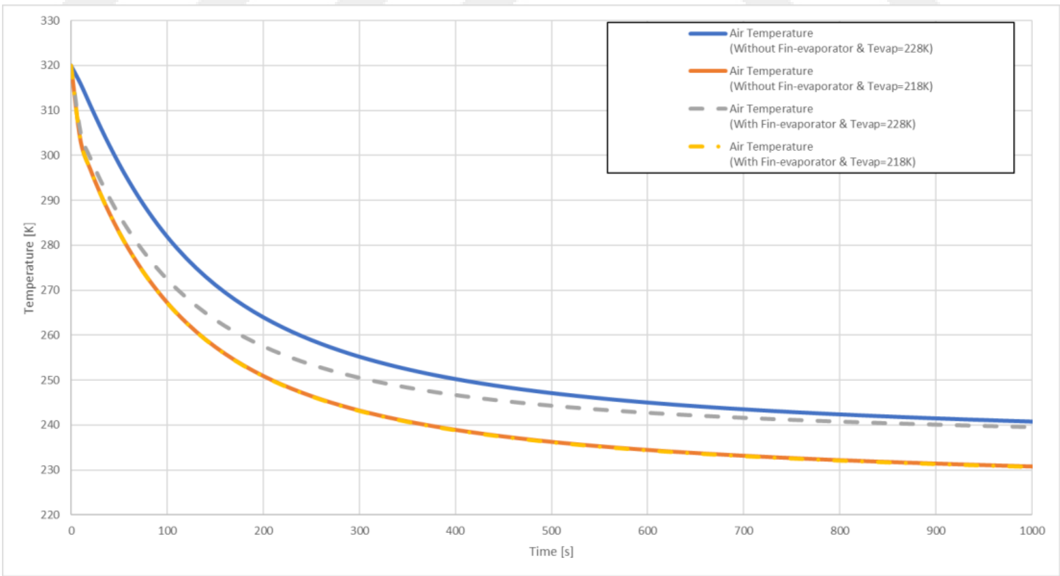

Figure 3.39 First 1000s overall air temperatures of 218K and 228K with and without fin on tube evaporator

The First 1000s were chosen as a specific time range to dedicate evaporator capacity, similarly, there is a closer view in Fig 3.39. This result proves that 228K and with the fin on tube evaporator system has the highest cooling rate. For 228K, delta temperature with and without fin on tube evaporator was 1.2K, it's even less than this for 218K. Finally, we can dedicate that fin on tube evaporator has a positive effect on drying/dehumidification in the vacuum process as well as in terms of cooling.

3.6 Transient Flow Analysis of Cooling Volume

In the cooling volume flow analysis, only the air volume of the cabin was modeled. Since flow analysis is more complex in such numerical models, it was aimed to obtain a simpler model. The simplified model steps obtained for the cooling volume flow analysis are presented in Fig 3.40.

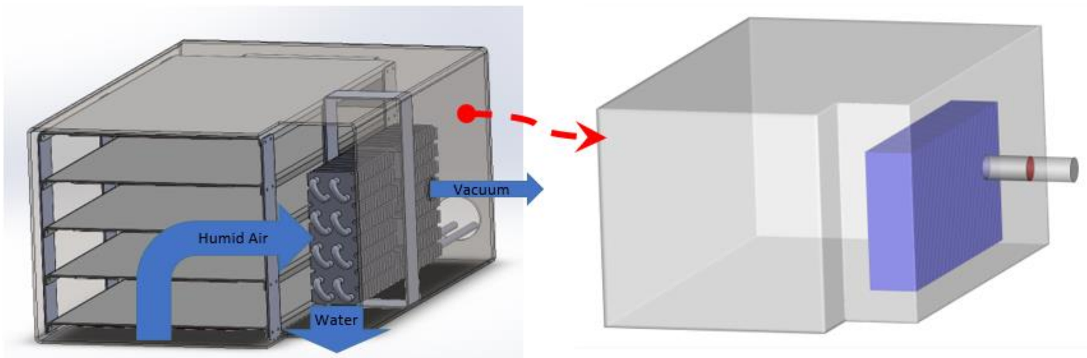

Figure 3.40 Transient CFD flow analysis of cooling volume

The blue part is the fin on tube model and pipe is simulated pressure drop by the vacuum pump. Air volume, volume outlet surface, and fins are shown in Fig 3.41. Mesh details are shown in Fig 3.42.

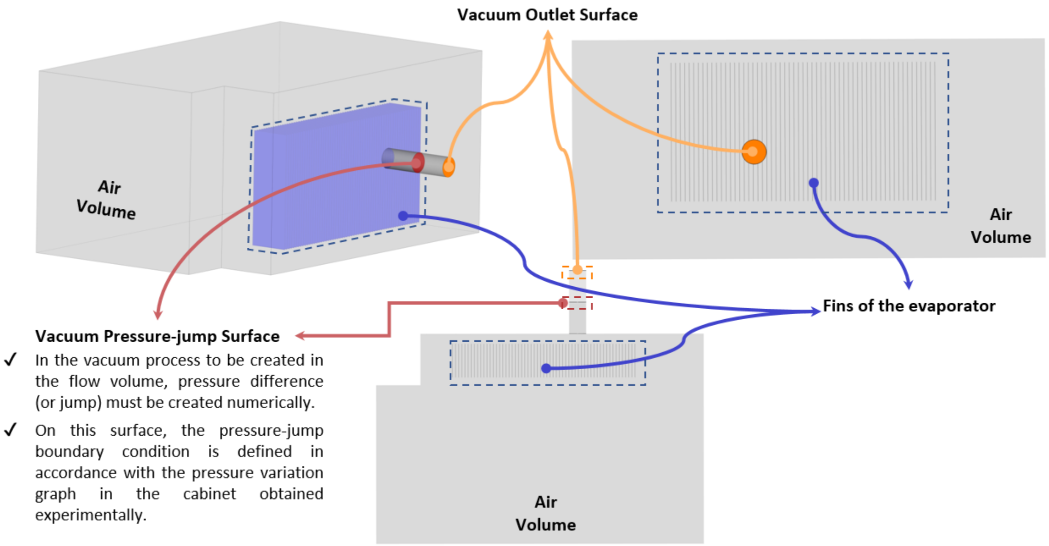

Figure 3.41 Air volume, volume outlet surface, and fin of the evaporator in CFD model

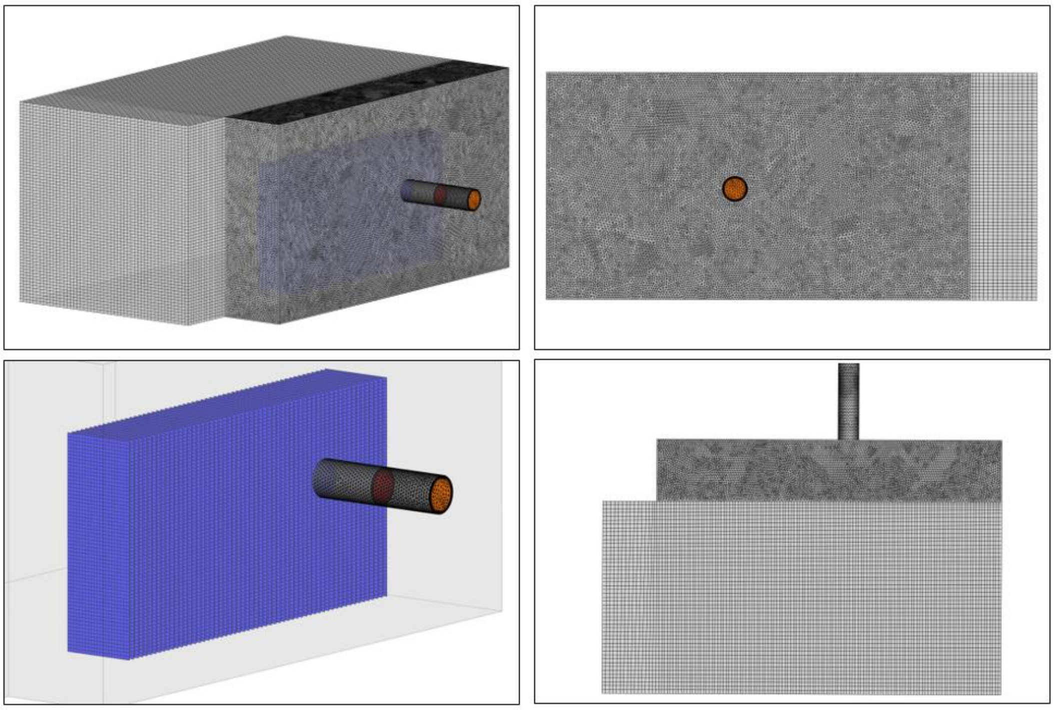

Figure 3.42 Mesh details for transient flow analysis

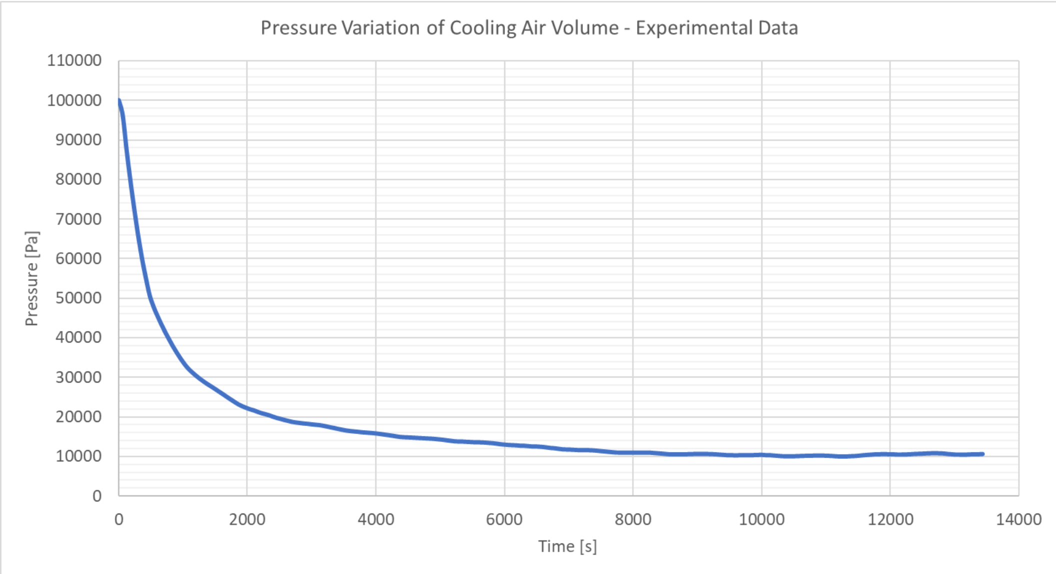

Figure 3.43 Experimental data pressure drop

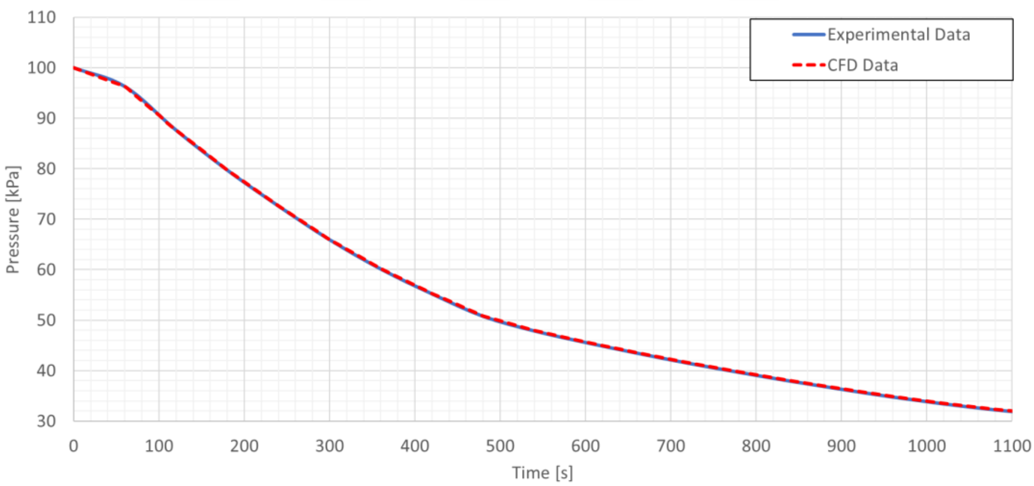

Figure 3.44 Pressure variation of cooling volume from experimental data

Experimental pressure drop is shown in Fig. 3.43. According to this result approximate pressure jump (68kPa) was applied to the red surface shown in Fig 3.41 to simulate the vacuum process. Experimental and the CFD results outputs are aligned and shown in Fig 3.44.

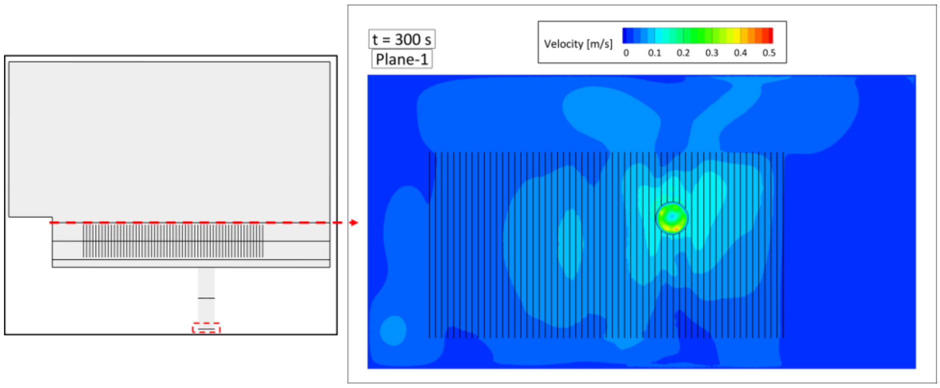

(a)

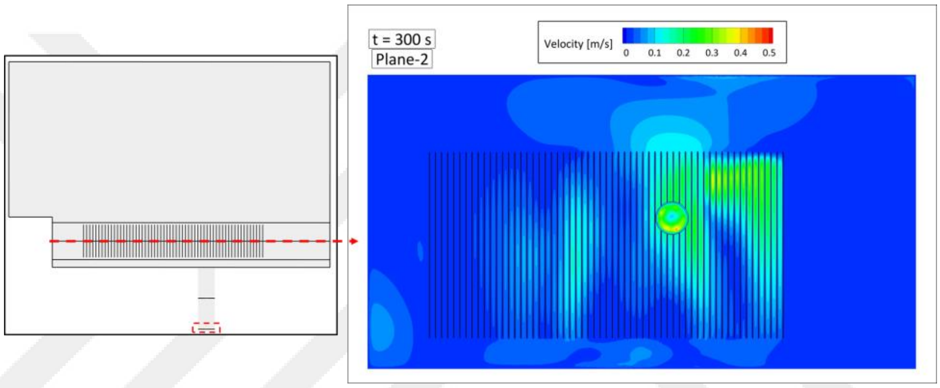

(b)

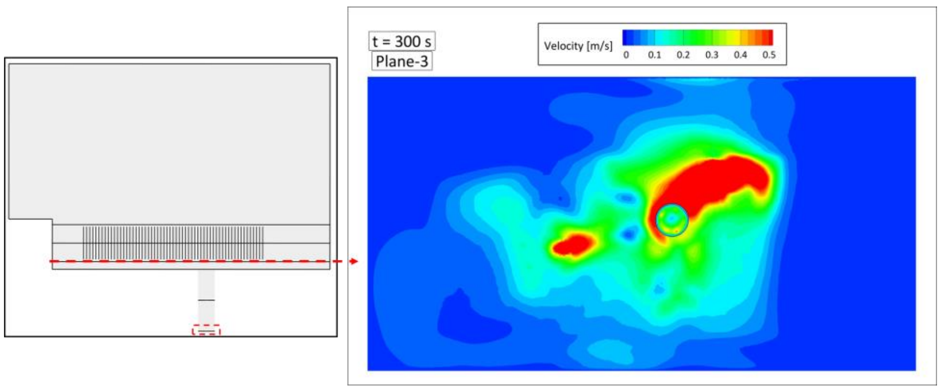

(c)

Figure 3.45 Velocity streamlines around fin on tube evaporator for 300s

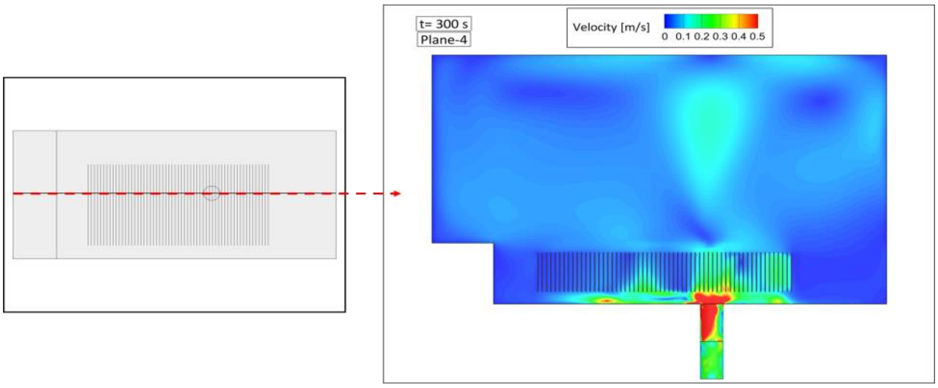

(d)

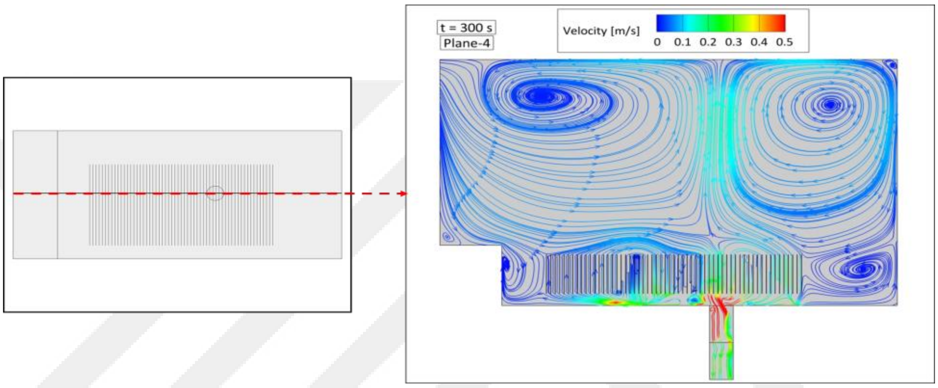

(e)

Figure 3.45 Continues

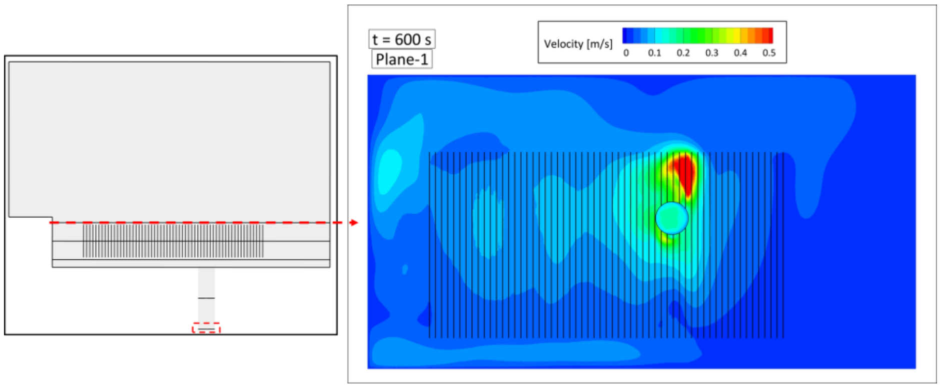

(a)

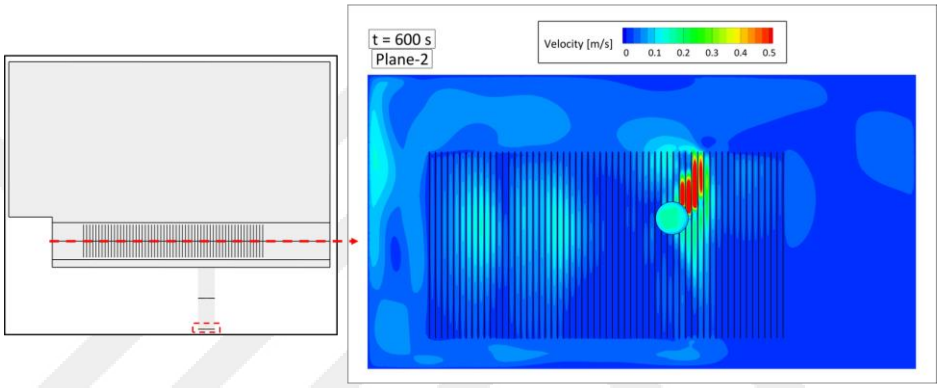

(b)

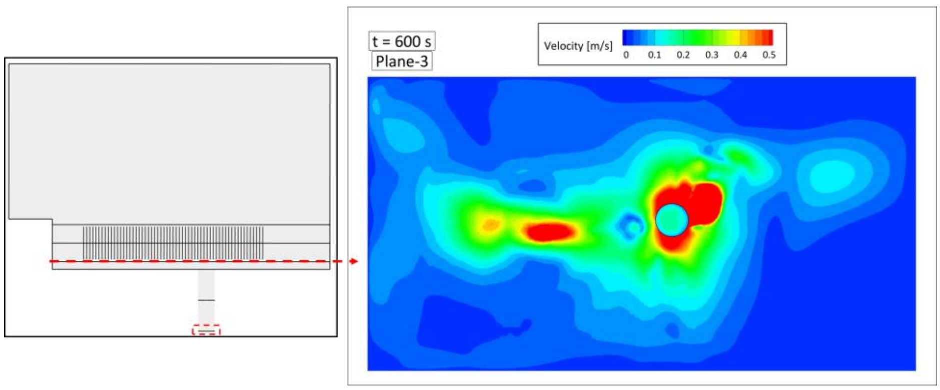

(c)

Figure 3.46 Velocity streamlines around fin on tube evaporator for 600s

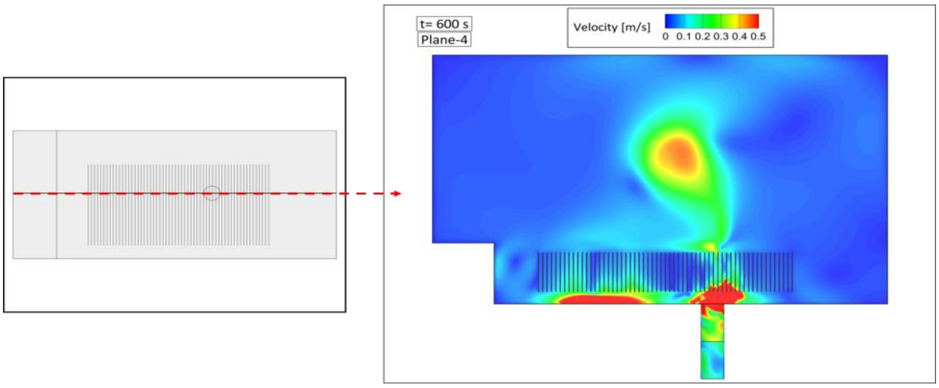

(d)

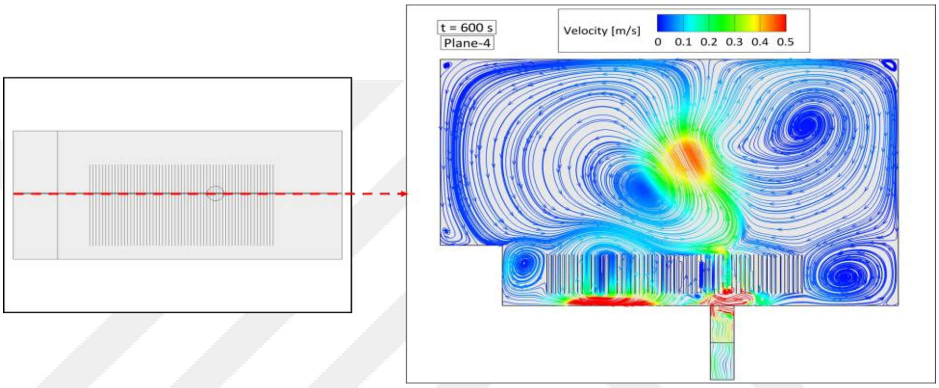

(e)

Figure 3.46 Continues

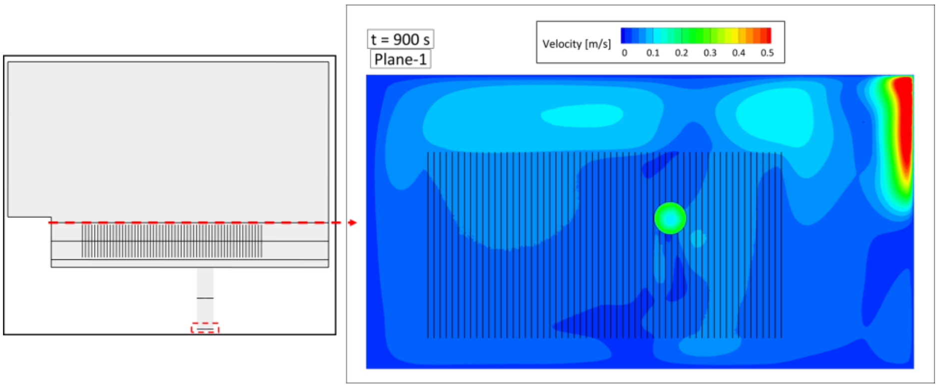

(a)

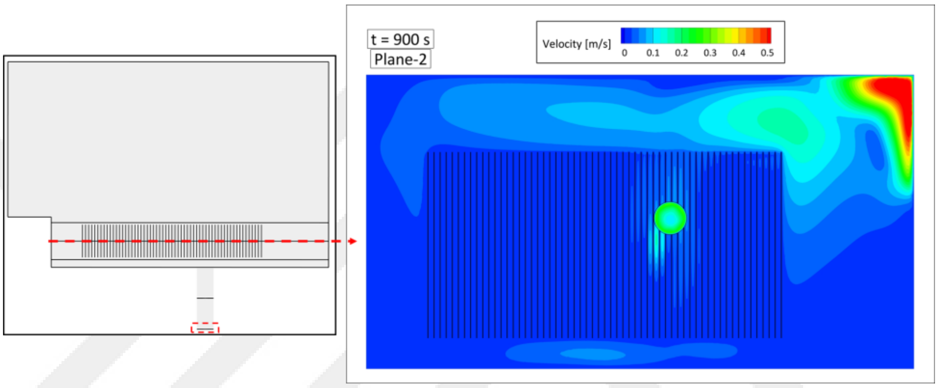

(b)

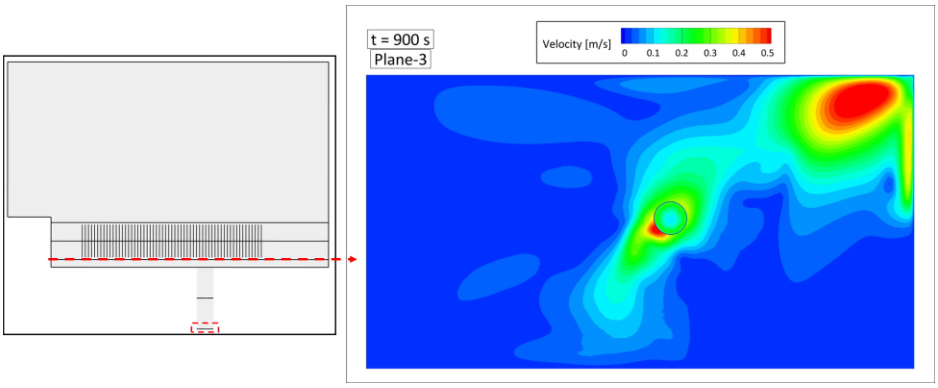

(c)

Figure 3.47 Velocity streamlines around fin on tube evaporator for 900s

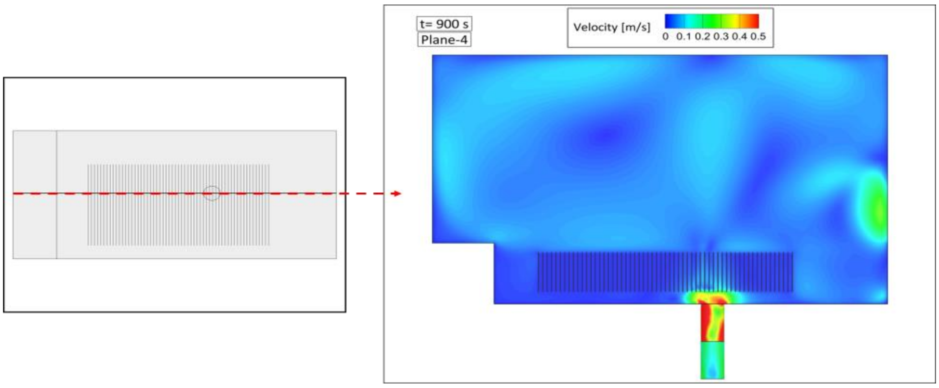

(d)

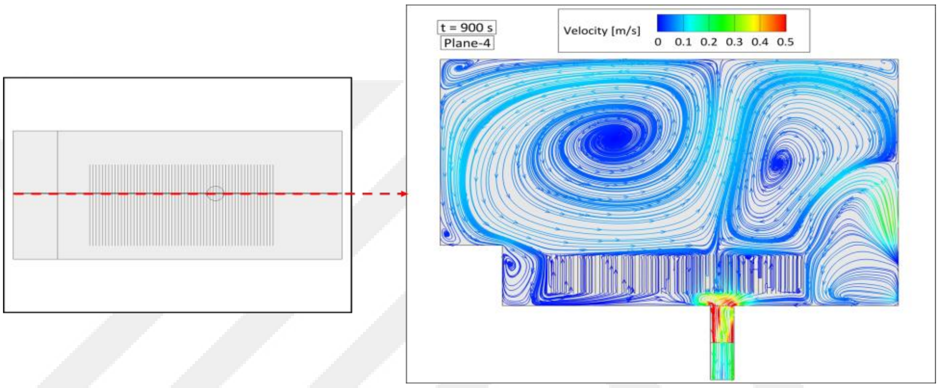

(e)

Figure 3.47 Continues

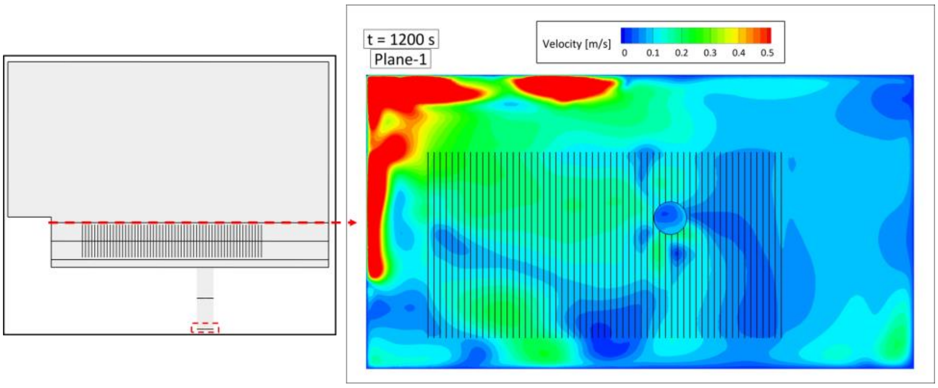

(a)

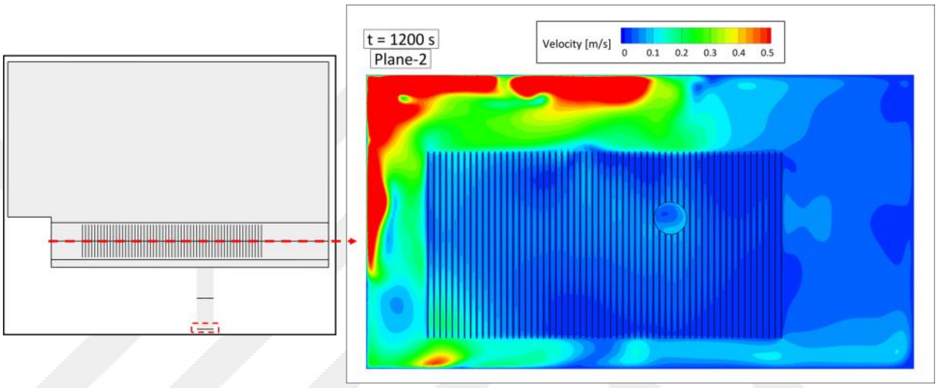

(b)

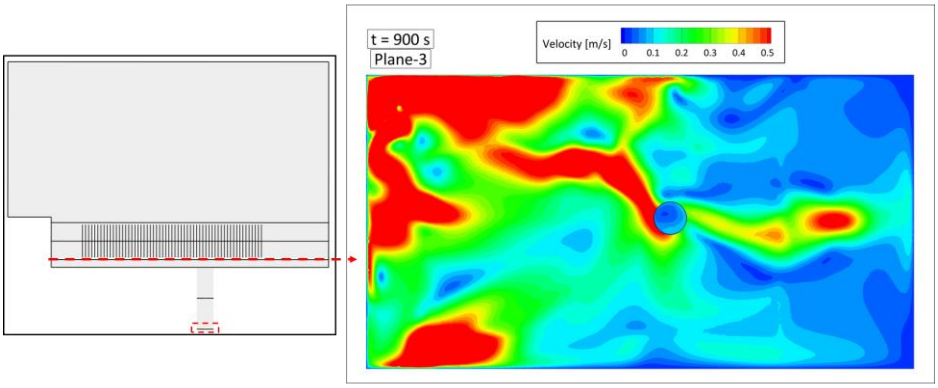

(c)

Figure 3.48 Velocity streamlines around fin on tube evaporator for 1200s

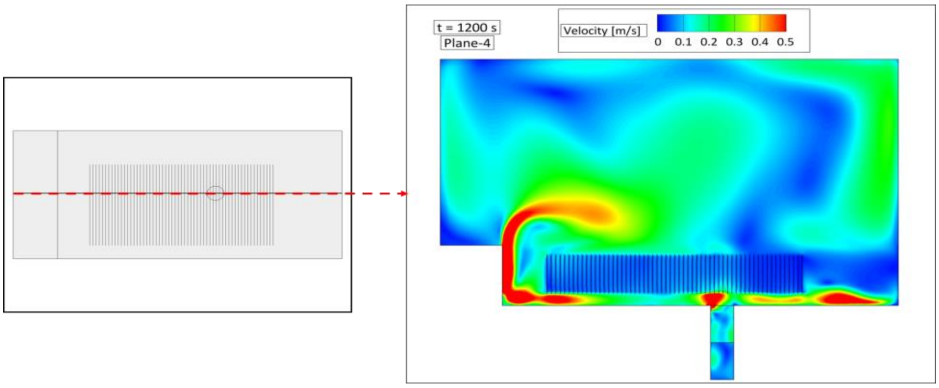

(d)

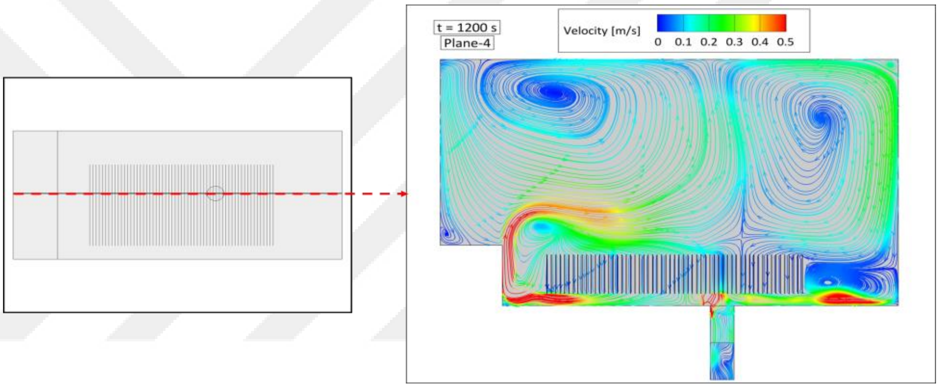

(e)

Figure 3.48 Contimıes

Considering the airflow passing through the fin on tube evaporator, there is intense flow in the sections close to the vacuum channel and homogeneous flow in the other sections. Similarly, the highest speed value compared to other sections was found in the fin-evaporator fins close to the vacuum channel. In the streamline graphics obtained with the top view and the velocity contours, the air cycles between the wings on the left. Thus, the air interacts with the fins of the fin on tube evaporator for a longer time before the air exit through the vacuum channel and has a positive contribution to the dehumidification application.

In order to achieve homogeneity in terms of velocity distribution and air passage between fin-evaporator fins, it is recommended to shift the position of the vacuum channel and fin-evaporator fins to the left a little more compared to the top view which is shown in Fig 3.49

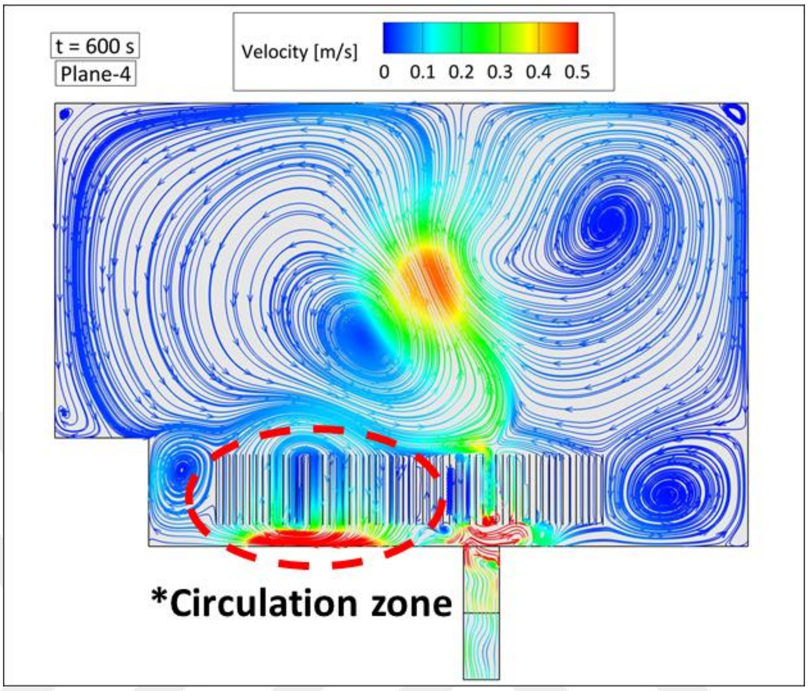

Figure 3.49 Circulation zone

CHAPTER FOUR
CONCLUSIONS

In this study, the freezing stage was modeled and analyzed with a TECM method. The Crank-Nicholson method was used for accurate results in Matlab. The gradual working logic was taken from the real system while the first design period. The single-step working logic was calculated based on gradual working logic. Different working logics were investigated with different conditions and results were compared accordingly. A rectangular design was investigated as a proposal design. Displacements were compared with different ideas and compared with the cylindrical chamber. Also, to improve the performance of the machine, there were some scenarios to improve the air circulation around the cooling system of the machine. The machine CFD model was created and analyzed with proposal outer and inner design points. In order to better cooling performance, foam and chamber were modeled to find better foam thickness, evaporator temperature, and fin on tube evaporator benefits, the results can be summarized as follows:

- Gradual and single-step working logics were analyzed with the TECM method on Matlab2020b. Single-step working logic was calculated based on the average temperature of the stabilized temperature during the last 10h of gradual working. Results showed that internal air and insulation temperatures were similar, lower than 1.5K but the product core temperature was 4.15K colder with gradual working. The reason is the compressor has lower pressure and colder temperatures which helps to achieve a lower temperature of the product.

- The capacity is another key point that shows the machine's performance. In this case, different weights; 3kg, 4kg, and 5kg were simulated with gradual and singles-step working logic. Results showed that lower temperatures can achieve with less weight. Increasing the weight also increases the thermal resistance between air and product core for that reason it's hard to achieve colder temperatures with high weights.

- The absorbed heat showed the heat capacity of the parts and the product has the bigger heat capacity for both working logic. The reason is product specific heat is higher than air and insulation. There are fluctuations with gradual working logic, the reason is the temperature change fluctuations and it affected the absorbed heat.

- Evaporator capacity is an important point at the design stage and evaporator capacity is calculated as the sum of the left and right sides of the electrical scheme. The time parameter was taken approximately 10 minutes to eliminate the first resistance of the chamber and other metal parts. The evaporator capacity can be 150W for better and safer cooling performance.

- A rectangular chamber was proposed as a new design with some improvements such as a fin on tube evaporator. The purpose of the fin on tube evaporator is the eliminate the humidity and help with cooling performance.

- The fin on tube evaporator was placed to the right of the chamber and this empty cavity was weak area in terms of displacements. For that reason, there was some design improvement like support and a thicker chamber. Results were compared with the cylindrical chamber and a 2mm thickness chamber with two supports was the best option in the sense of durability and economic reason.

- Customers mostly put the machine in the middle of the furniture and it affects the cooling performance. In order to improve air circulation, front and backward air grills were added, and also diffuser, and separator parts were added to insulate the compressor condenser part from the chamber. The best option was the air grills with the separators. Chamber wall temperatures are colder with diffuser and separator, only the top wall is hotter cause the hot air was leaved from the backward grill and flows through the top wall.

- Insulation thickness and evaporator temperatures are crucial for cooling performance. Steady-state thermal analyses were done at 245K and 255K with

40mm,45mm, and 50mm insulation thickness. Heat gains differences are 40mm to 45mm with %6, and 45mm to 50mm with %8.

- The fin on the evaporator was placed to eliminate humidity during the vacuum period since it helped cooling performance. Evaluate the fin on tube evaporator benefit, evaporator temperature 218K and 228K analyzed with and without fin on the evaporator. Experimental results were compared with the CFD simulations. Temperatures can compare with air temperatures. They have similar results for all options. Heat storage showed for all scenarios and they were very similar. Another important point was the calculation of the evaporator capacity with the CFD method. The evaporator capacity was 160W for 218K with the fin on tube evaporator and 160.8W, without the fin on tube evaporator is 160.36W. We calculated evaporator capacity 150W with the TECM method and the results showed the similarity of TECM and CFD methods in terms of evaporator capacity.

- Another purpose of the fin on tube evaporator was the eliminate humidity but air should pass through the fin on tube evaporator. Transient flow analyses were done to observe air flows during the vacuum process. Air circulation streams and velocity were evaluated for 300, 600, 900, and, 1200 seconds. There was a circulation zone between the evaporator and the lateral wall of the chamber.

REFERENCES

Deconinck, A. H., & Roels, S. (2016). Comparison of characterisation methods determining the thermal resistance of building components from onsite measurements. *Energy and Buildings*, *130*, 309–320.

Dube Kerme, E., & Fung, A. S. (2020). Transient heat transfer simulation, analysis and thermal performance study of double U-tube borehole heat exchanger based on numerical heat transfer model. *Applied Thermal Engineering, 173*, 115189

Gan, Y., Wang, J., Liang, J., Huang, Z., & Hu, M. (2020). Development of thermal equivalent circuit model of heat pipe-based thermal management system for a battery module with cylindrical cells. *Applied Thermal Engineering, 164,* 114523.

Ghiaus, C., & Ahmad, N. (2020). Thermal circuits assembling and state-space extraction for modelling heat transfer in buildings. *Energy, 195*, 117019.

Greco, A., Cao, D., Jiang, X., & Yang, H. (2014). A theoretical and computational study of lithium-ion battery thermal management for electric vehicles using heat pipes. *Journal of Power Sources, 257*, 344–355.

Gunes N. Ç., E. O. (2017, April 19-22). Vakum soğutma tekni̇ği̇ni̇n fesleğen için incelenmesi [Bildiri Özeti]. On Üçüncü Ulusal Tesisat Mühendisliği Kongresi, Soğutma Teknolojileri Sempozyumu, İzmir, Türkiye

He, K. L., Chen, Q., Dong, E. fu, Ge, W. C., Hao, J. H., & Xu, F. (2018). An improved unit circuit model for transient heat conduction performance analysis and optimization in multi-layer materials. *Applied Thermal Engineering, 129*, 1551–1562.

Ho, C. J., Huang, C. S., & Viskanta, R. (2015). A thermal circuit model consistent with integral energy balance for internal forced convection in a circular tube. *International Journal of Heat and Mass Transfer, 87*, 409–417.

Ishizuka, M., Hatakeyama, T., Funawatashi, Y., & Koizumi, K. (2011). Application of thermal network model to transient thermal analysis of power electronic package substrate. *Active and Passive Electronic Components, 823654*.

Isik, E. (2007). Comparison of the thermodynamically analysis of vacuum cooling method with the experimental model. *American Journal of Food Technology, 2*(4), 217–227.

Jin, T. X. (2007). Experimental investigation of the temperature variation in the vacuum chamber during vacuum cooling. *Journal of Food Engineering, 78*(1), 333–339.

Konky, P., Balmer, R., Keat, W., Wise, G., (2013). The Elements of Thermal Design. *Exploring Engineering (3rd ed.,* pp. 258-281).

Liu, Y., Li, G. H., & Jiang, L. X. (2010). A new improved solution to thermal network problem in heat-transfer analysis of spacecraft. *Aerospace Science and Technology, 14*(4), 225–234.

Lomeiko, O., Yefimenk, L., & Tarasenko, V. (2019). Vacuum Cooling Technology for Pre-cooling of Cherry Fruits. *Modern Development Paths of Agricultural Production*, 281-288

Marcotte, B., & Bernier, M. (2019). Experimental validation of a TRC model for a double U-tube borehole with two independent circuits. *Applied Thermal Engineering, 162*, 114229.

Mc Donald, K., Sun, D. W., & Lyng, J. G. (2002). Effect of vacuum cooling on the thermophysical properties of a cooked beef product. *Journal of Food Engineering, 52*(2), 167–176.

Mutlu Ozturk, H., Ozturk, H. K., & Kocar, G. (2011). Comparison of vacuum cooling with conventional cooling for purslane. *International Journal of Food Engineering, 7*(6).

Nguyen, A., & Elsami-Nejad, P. (2019). A transient coupled model of a variable speed transcritical CO2 direct expansion ground source heat pump for space heating and cooling. *Renewable Energy, 140*, 1012–1021.

Pau, D. S. ., Fleischmann, C. M., Spearpoint, M. J., & Li, K. Y. (2009). Thermophysical properties of polyurethane foams and their melts. *Fire and Materials, 38*, 433-450

Prasad, K., Kramer, R., Marsh, N., Nyden, M., Ohlemiller, T., & Zammarano, M. (2009). Numerical simulation of fire spread on polyurethane foam slabs. *Conference Proceedings - Fire and Materials, 11th International Conference and Exhibition.*

Ramaswamy, H. S., & TUNG, M. A. (1981). Thermophysical Properties of Apples in Relation to Freezing. *Journal of Food Science, 46*(3), 724–728.

Sun, D. W., & Hu, Z. (2003). CFD simulation of coupled heat and mass transfer through porous foods during vacuum cooling process. *International Journal of Refrigeration, 26*(1), 19–27.

Wang, L., & Sun, D. W. (2001). Rapid cooling of porous and moisture foods by using vacuum cooling technology. *Trends in Food Science and Technology, 12*(5–6), 174–184.

Wang, L., Yan, J., Wang, C., & Li, X. (2017). Numerical study on optimization of ejector primary nozzle geometries. *International Journal of Refrigeration*, *76*, 219-229.

Wang, S., & Xu, X. (2006). Simplified building model for transient thermal performance estimation using GA-based parameter identification. *International Journal of Thermal Sciences*, *45*(4), 419–432.

Watanawanavet, S. (2005). *Optimization of a high-efficiency jet ejector by computational fluid dynamic software*. Phd Thesis, A&M University, Texas.

Wu, H., Liu, Z., Han, B., & Li, Y. (2014). Numerical investigation of the influences of mixing chamber geometries on steam ejector performance. *Desalination*, *353*, 15-20.

Wu, Y., Zhao, H., Zhang, C., Wang, L., & Han, J. (2018). Optimization analysis of structure parameters of steam ejector based on CFD and orthogonal test. *Energy*, *151*, 79-93.

Yapıcı, R., Ersoy, H. K., Aktoprakoğlu, A., Halkacı, H. S., & Yiğit, O. (2008). Experimental determination of the optimum performance of ejector refrigeration system depending on ejector area ratio. *International Journal of Refrigeration*, *31*(7), 1183-1189.

Zhang, S. W., Talib, A. R. A., Mokhtar, A. S., & Kamal, S. M. M. (2009). Design improvement in vacuum cooling system. *International Journal of Engineering and Technology*, *6*(1), 51–59.

Zhao, R., Gosselin, L., Fafard, M., & Ziegler, D. P. (2013). Heat transfer in upper part of electrolytic cells: Thermal circuit and sensitivity analysis. *Applied Thermal Engineering*, *54*(1), 212–225.

Zhao, S. Y., & Chen, Q. (2016). A thermal circuit method for analysis and optimization of heat exchangers with consideration of fluid property variation. *International Journal of Heat and Mass Transfer*, *99*, 209–218.

Zhu, Y., & Jiang, P. (2014). Experimental and numerical investigation of the effect of shock wave characteristics on the ejector performance. *International Journal of Refrigeration*, *40*, 31-42.

Zhu, Y., Cai, W., Wen, C., & Li, Y. (2009). Numerical investigation of geometry parameters for design of high performance ejectors. *Applied Thermal Engineering*, *29*(5-6), 898-905.

Zilio, C., Brown, J. S., Schiochet, G., & Cavallini, A. (2011). The refrigerant R1234yf in air conditioning systems. *Energy*, *36*(10), 6110-6120.